COST-EFFECTIVENESS ANALYSIS OF ^{68}GA-NODAGA-EXENDIN-4 PET/CT FOR LOCALIZING INSULINOMAS

MASTER THESIS INDUSTRIAL ENGINEERING AND MANAGEMENT

M.J.E. GRAMSBERGEN, S2644487

07-07-2023

UNIVERSITY OF TWENTE.

Summary

Introduction:
This cost-effectiveness analysis was performed to determine if a diagnostic pathway for patients with adult endogenous hyperinsulinemic hypoglycemia (AHH) incorporating ^{68}Ga-NODAGA-exendin-4 PET/CT (from now on referred to as Exendin) would be a cost-effective alternative to the Dutch current standard of care diagnostic pathway, CT-MRI-EUS-DOTA. This indicates a diagnostic pathway in which the patient encounters these imaging techniques in this order. Exendin is an imaging technique aimed at localizing insulinomas, which are neuroendocrine tumors that can form in the pancreatic beta cells and which can cause AHH.
Methods:
The cost-effectiveness of diagnostic pathways incorporating Exendin was assessed using a discrete event simulation (DES) model written in R. The model was populated mainly using patient-level data from Boss *et al.*, 2019 on patients who underwent surgery after having their insulinoma localized via various imaging techniques, including the experimental Exendin. The dataset provided data on imaging technique diagnostic accuracy, as well as quality-of-life (QoL) scores for patients. Additional data was retrieved via literature research and via interviews with experts. The DES model simulated hypothetical patients and tracked their time in the model, their cost and their quality-adjusted life years (QALYs). In the DES model, the Dutch current standard of care diagnostic pathway, consisting of conventional imaging techniques, was compared to four experimental diagnostic pathways. These experimental diagnostic pathways were adaptations of the standard diagnostic pathway, with Exendin at different time points. This resulted in four experimental diagnostic pathways: Exendin+CT-MRI-EUS, CT-Exendin-MRI-EUS, CT-MRI-Exendin-EUS and CT-MRI-EUS-Exendin. DOTA could not be implemented in the experimental diagnostic pathways, due to there not being enough patient data to determine the conditional probability of DOTA. Using the DES model, a probabilistic sensitivity analysis (PSA) was performed. Using the PSA output, the average net monetary benefit (NMB) was estimated for willingness to pay (WTP) thresholds ranging from €0-€100.000. The diagnostic pathway with the highest average NMB at the relevant Dutch WTP threshold of €20.000 per QALY gained was deemed the most cost-effective diagnostic pathway. In addition, a deterministic sensitivity analysis (DSA) was performed to see how varying different model parameters impacted the cost-effectiveness outcomes.
Results:
The experimental diagnostic pathway CT-MRI-Exendin-EUS was found to have the highest average NMB at the relevant WTP threshold of €20.000/QALY at €88.601. The current standard of care diagnostic pathway, CT-MRI-EUS-DOTA, had an average NMB of €88.396. Comparing CT-MRI-Exendin-EUS to the current standard of care, the incremental costs were -€200 and the QALYs were comparable. The next best alternative diagnostic pathway CT-Exendin-MRI-EUS had an average NMB of €88.480. Comparing CT-Exendin-MRI-EUS to CT-MRI-Exendin-EUS, the incremental costs were €152 and the QALYs were similar.
Conclusion:
The diagnostic pathway CT-MRI-Exendin-EUS was estimated the most cost-effective in this analysis.
Discussion:
The results of this study suggest that revising the current diagnostic approach for AHH patients within the Dutch healthcare system might be beneficial. However, it's important to acknowledge the limitations of the data used in this study, as it was derived from a relatively small patient group. The model's time horizon was also relatively short, lasting only 2000 days, and did not extend to the patients' end of life. In addition, the QoL gains achieved by Exendin by having less patients with an insulinoma leave the diagnostic pathway without having their insulinoma localized, were not accounted for in this analysis. Consequently, the full extent of the positive effect of Exendin on patients' QoL may not have been fully captured. For a more precise estimate of the cost-benefit of incorporating Exendin into the diagnostic pathway, it would be advisable to expand upon this analysis. This extension should aim to address and resolve the limitations mentioned in this section, as these were estimated to have the largest impact on the cost-effectiveness outcomes of this analysis.

Table of contents

1. Introduction

In this report, the outcomes of a cost-effectiveness analysis of the localization of insulinomas using ^{68}Ga-NODAGA-exendin-4 PET/CT (from now on referred to as Exendin) are presented and discussed. Insulinomas are neuroendocrine tumors that can form in the pancreatic beta cells. They are rare, given their incidence of 1-4 people per million per year, but are the most common cause of adult endogenous hyperinsulinemic hypoglycemia (AHH) (Okabayashi *et al.*, 2013; Placzkowski *et al.*, 2009; Richards *et al.*, 2002). In patients, AHH can produce symptoms such as confusion, diplopia, dizziness and in severe cases even seizures or loss of consciousness (Kinova, 2015; Senniappan *et al.*, 2012).

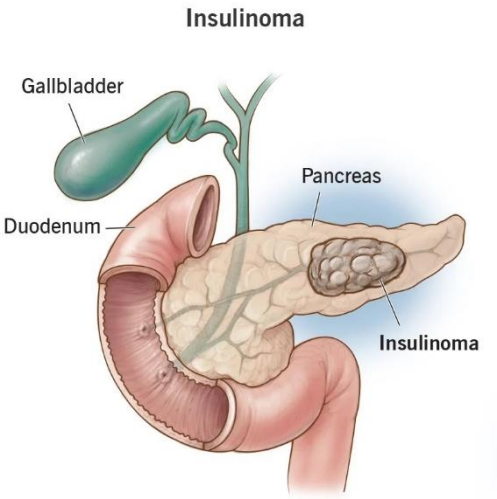

Figure 1: illustration of an insulinoma (Cleveland Clinic, 2021)

For a patient to be diagnosed with AHH, a positive prolonged fasting test must be administered. If the test result is positive, the localization of the insulinoma(s) is performed with one or multiple techniques. In case non-invasive imaging techniques like computed tomography (CT) and magnetic resonance imaging (MRI) fail to localize the insulinoma, alternative and invasive imaging techniques are deployed, such as endoscopic ultrasound (EUS). Most insulinomas are benign (more than 90%) and therefore the preferred surgery types are pancreas-preserving (Richards *et al.*, 2002). To enable these pancreas preserving procedures, knowing the precise location of the insulinoma is essential.

The imaging technique that plays a central role in this analysis, is the Exendin imaging technique. Recently, a study was performed by Boss *et al.*, 2019 that explored the accuracy of Exendin for localization of insulinomas in 69 patients with proven AHH, compared to individual current routine imaging techniques: CT, MRI, EUS, PET/CT with ^{68}Ga-DOTATOC or ^{68}Ga-DOTATATE (both techniques combined will be referred to as DOTA from now on) and EUS. For these figures, the researchers only considered patients in which an insulinoma was actually found during surgery afterwards. The accuracy thus reflects the percentage of confirmed insulinomas an imaging technique was able to localize. The results of this study were in favor of Exendin, as can be seen in table 1 below:

Table 1: accuracy of Exendin as compared to current non-invasive imaging techniques (Boss et al., 2019)

	Accuracy	**95% CI**
Exendin	96.2%	87.3-98.8%
DOTA	62.2%	48.7-74.1%
CT	72.5%	57.1-83.9%
MRI	70.3%	54.1-82.5%
EUS	79.3%	61.4-90.1%

At first glance, these results look promising for the application of Exendin, but diagnostic performance is not the only matter of importance in healthcare. The consequences of (in)correctly diagnosing disease and the cost aspect are just as relevant. Healthcare is becoming more and more expensive and in the Netherlands, the cost of healthcare will increase from 11% of the GDP in 2025 to 18% of the GDP by 2060 (Aalbers *et al.*, 2022). Because of these considerable financial challenges, healthcare providers have to be more and more aware of the costs of treatment options and therefore have to make decisions that are increasingly cost driven. For these cost driven decisions, healthcare providers heavily rely on cost-effectiveness analyses, in which the cost-effectiveness of experimental healthcare interventions is determined.

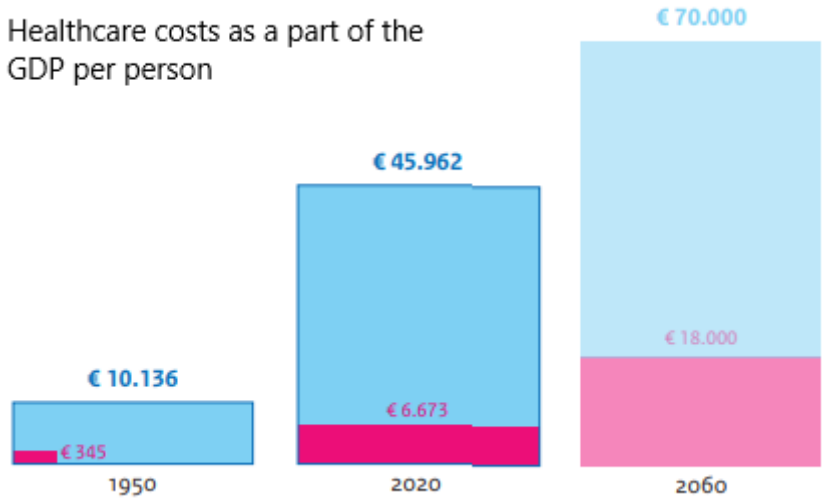

Figure 2: healthcare costs in the Netherlands are steadily increasing (Aalbers et al., 2022)

Exendin could become part of what's called a diagnostic pathway, which is the pathway a patient diagnosed with AHH would follow to have a potential insulinoma localized. In this case it contains a number of imaging techniques that the patient can encounter in a predetermined order. The cost-effectiveness can thus not be found specifically for an individual imaging technique, but for the diagnostic pathway it is included in. This analysis considers the impact on the full pathway the patient follows, also taking the impact of the diagnosis on treatment into consideration.

In order to find whether a diagnostic pathway that includes Exendin would be more cost-effective than the current diagnostic pathway, a discrete-event simulation (DES) model was built in R. The model determines the net monetary benefit (NMB) of the currently standard diagnostic pathway, as well as the NMB of a number of diagnostic pathways that do include Exendin. If a diagnostic pathway with Exendin is found to have an average NMB that is the highest out of all diagnostic pathways at the relevant willingness-to-pay (WTP) threshold, then that diagnostic pathway may be deemed the most cost-effective diagnostic pathway for patients with AHH, of course considering all relevant modeling limitations.

2. Background

In this chapter, background information is given on the analysis. An introduction is provided on insulinomas, the conventional and experimental imaging techniques and the surgery types. In addition, the medication types are described, as well as the polyclinic visits patients make.

2.1 Insulinomas

Insulinomas are neuroendocrine tumors that can form in the pancreatic beta cells. They are rare, given their incidence of 1-4 people per million per year, and are the most common cause of adult endogenous hyperinsulinemic hypoglycemia (AHH) (Okabayashi *et al.*, 2013; Placzkowski *et al.*, 2009; Richards *et al.*, 2002). AHH is a condition in which the body experiences either chronic or episodes of low blood glucose levels due to excessive endogenous insulin production in the pancreas. The excessive endogenous insulin production is thus often caused by neuroendocrine tumor(s) like insulinomas. AHH can cause symptoms such as confusion, diplopia, dizziness and in severe cases even seizures, loss of consciousness or (in case of metastasis) even death (Kinova, 2015; Senniappan *et al.*, 2012).

Although insulinomas can develop at any age, globally the average population's age-specific incidence peak occurs in the fifth decade of life (Goswami *et al.*, 2012; Jensen *et al.*, 2012; Öberg, 2010). Insulinomas occur in the pancreas with equal distribution over its parts (Kinova, 2015). They occur far more often as benign, with less than 10% being malignant and they are mostly solitary (De Herder *et al.*, 2011; Ferrer-Garcia *et al.*, 2013; Tucker *et al.*, 2006). They are also typically small, with 90% being smaller than 2 cm (Mehrabi *et al.*, 2014; Okabayashi *et al.*, 2013).

Because of the mostly benign nature of insulinomas, the preference for surgery often lies with pancreas-preserving techniques (Richards *et al.*, 2002). The different relevant surgery types are discussed in section 2.4 on Surgery types.

2.2 Conventional imaging techniques for localization

A patient with an insulinoma almost always undergoes surgery, but it is paramount that the insulinoma is localized beforehand. Preoperative imaging is helpful for a number of reasons, including tumor localization, disease severity assessment, selecting the best surgical strategy for a successful first resection, and further treatment planning (Kinova, 2015). To familiarize the reader with the conventional imaging techniques mentioned in this report, a short overview and description of said imaging techniques is provided in this section.

2.2.1 CT

A computed tomography (CT) scan is a medical imaging procedure that uses x-rays and computer technology to create detailed images of the inside of the body. Unlike traditional x-ray imaging, which only produces a single image, a CT scan produces a series of cross-sectional images, which can be viewed in different planes. This allows the physician to see

structures inside the body in greater detail and with more accuracy than traditional x-ray images. For insulinoma, the CT may visualize the location and potential metastasis, but also the relationship to other structures (Kinova, 2015). Before surgery, a CT is actually required to provide the surgeon with an anatomical overview of the internal organs and their orientations (Boss *et al.*, 2019). The procedure itself is usually painless and typically takes between 15 and 30 minutes. It is non-invasive, radiation exposure is low but not zero, typically done with contrast medium and the patient may experience mild discomfort due to the compression of the area being scanned.

Figure 3: CT scan (left) and MRI scan (right)

2.2.2 MRI

A magnetic resonance imaging (MRI) scan is a medical imaging procedure that uses a large magnet, radio waves, and computer technology to produce detailed images of the inside of the body. Unlike a CT scan, which uses x-rays to create images, an MRI scan does not use ionizing radiation. Instead, it relies on the magnetic properties of certain atoms in the body to produce detailed images of the body's internal structures.

For insulinoma, the MRI scan could visualize its location and potentially reveal metastasis (Kinova, 2015). The procedure itself typically takes between 30 and 60 minutes, and the patient is required to lie still on a table that is moved into the magnet. The patient will need to wear earplugs or headphones to protect their hearing from the loud noise that the machine makes.

A large disadvantage is that it is not useful in cases that the patient has metal on their body, such as a pacemaker, aneurysm clip, artificial joint, cochlear implant, etc. Since the scan is conducted in a confined space, it may trigger a claustrophobic episode (an intense fear of closed spaces) in some individuals.

2.2.4 ^{68}Ga-DOTATOC and ^{68}Ga-DOTATATE (DOTA-SSA-PET/CT)

^{68}Ga-DOTATOC and ^{68}Ga-DOTATATE (also known as DOTA-SSA-PET/CT) are types of PET tracers used in the diagnosis and treatment monitoring of neuroendocrine tumors and other related tumors, such as pituitary tumors and pheochromocytomas. DOTATOC and DOTA-SSA are specific type of somatostatin analogues that is attached to a chelator (DOTA) which

allows for the attachment of a radioactive isotope (in this case ^{68}Ga) for imaging purposes (Cox *et al.*, 2020; Hennrich *et al.*, 2020). The resulting products ^{68}Ga-DOTATOC and ^{68}Ga-DOTATATE are radiopharmaceuticals that bind to somatostatin receptors, which are overexpressed in insulinomas (Cox *et al.*, 2020; Hennrich *et al.*, 2020). By doing so, it allows the visualization and quantification of these tumors and also helps to identify the anatomic location of these tumors. As with most nuclear medicine imaging, the patient will be injected with the radiolabeled tracer, and then will wait for a certain period of time for the tracer to accumulate in the body. Then the patient will be scanned using a special camera that detects the gamma rays emitted by the tracer and creates detailed images of the distribution of the tracer in the body.

2.2.5 EUS

Endoscopic ultrasonography (EUS) is a medical procedure that combines the use of an endoscope, which is a thin, flexible tube with a light and camera on the end, and ultrasonography, which uses high-frequency sound waves to create images of the inside of the body (Caletti *et al.*, 1998). During an EUS procedure, the endoscope is inserted through the mouth or the rectum and advanced to the area of the body being examined, in this case the pancreas. The ultrasonic probe on the endoscope then generates sound waves, which bounce off the internal structures and are detected by the probe, creating images of the structures.

It is typically performed as an outpatient procedure, and it is generally safe and well-tolerated. The procedure takes about 30 minutes to complete, and the patient is usually sedated to minimize discomfort.

2.3 Exendin

As stated in the introduction, the imaging technique of interest for this report is Exendin. To familiarize the reader with this technique and its workings, a description of Exendin is provided in this section.

Exendin is a type of positron emission tomography (PET) tracer that is used in conjunction with a CT scan to produce detailed images of the inside of the body.

PET is a nuclear medicine imaging technique that involves the injection of a small amount of a radioactive tracer into the patient's body, in this case ^{68}Ga-NODAGA-exendin-4. This tracer is designed to bind selectively to the glucagon-like peptide-1 receptor (GLP-1R) using ^{68}Ga-labeled exendin-4, a stable analog of GLP-1, which selectively binds the GLP-1R with high affinity. The GLP-1R is particularly interesting, since 92% of benign insulinomas express high levels of this receptor (Reubi *et al.*, 2003). As the tracer decays, it emits positively charged particles called positrons. These positrons interact with electrons in the body to produce a type of radiation called gamma rays. A special camera is used to detect the gamma rays and create detailed images of the distribution of the tracer in the body. The detailed images in combination with the specific binding to GLP-1R allows the physician to tell the location of an insulinoma more easily.

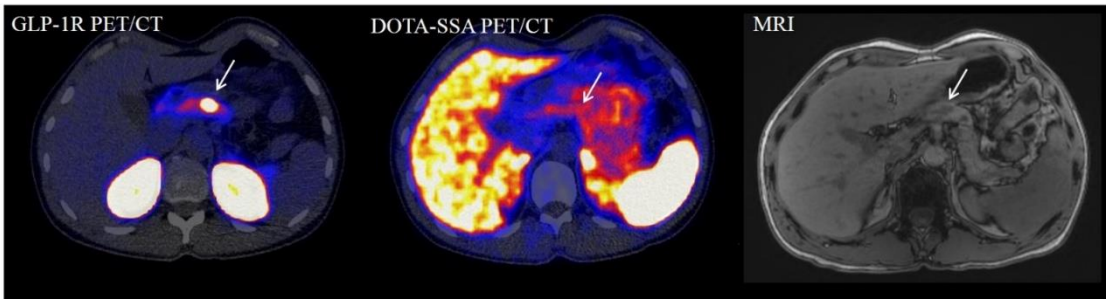

Figure 4: imaging produced by (from left to right) Exendin, DOTA-SSA-PET/CT and MRI (Boss et al., 2019)

2.4 Surgery types

Not all insulinomas and their locations are equal and there are multiple surgery types to account for this. To familiarize the reader with these surgery types, a short description is provided of said surgery types is provided in this section.

2.4.1 (Tail) resection

A (tail) resection is a surgical procedure, which typically involves an open surgery, which means that a large incision is made in the abdomen to access the pancreas. The surgeon will carefully identify the tumor before surgery using aforementioned imaging techniques. Once the tumor is located, the surgeon will carefully remove it, taking care not to damage the surrounding healthy tissue.

In some cases, the surgeon may also remove a small portion of the pancreas, called a "tail" resection, if the tumor is located in that area (Åkerström *et al.*, 2007). The tail of the pancreas is the portion of the pancreas that is closest to the spleen, it is not a critical area and removal of a small portion of it does not affect the function of the pancreas.

2.4.2 Enucleation

Enucleation is a minimally invasive procedure that is performed laparoscopically (through small incisions in the abdomen) using special instruments and a camera to guide the surgeon (Åkerström *et al.*, 2007; Rehman, 2011). During the procedure, the surgeon will make small incisions in the abdomen and insert a laparoscope, which is a thin, flexible tube with a light and camera on the end. The laparoscope is used to view the inside of the abdomen and locate the tumor.

Once the tumor is located, the surgeon will use special instruments to carefully remove the tumor, taking care not to damage the surrounding healthy tissue. The goal of the procedure is to remove the tumor while preserving as much healthy tissue as possible.

2.4.3 Whipple

The Whipple procedure, also known as a pancreaticoduodenectomy, is a surgical procedure that is used to treat insulinomas that are in the head of the pancreas. It is considered as a more complex and invasive procedure than enucleation, and it is typically reserved for larger or more aggressive tumors that cannot be safely removed through enucleation.

The procedure involves the removal of the head of the pancreas, the duodenum (the first part of the small intestine), the gallbladder, and possibly a portion of the common bile duct and stomach (Changazi *et al.*, 2020).

The surgery is done in two stages: first, the surgeon will perform a pylorus-preserving pancreaticoduodenectomy, which is a more complex version of the Whipple procedure that preserves the connection between the stomach and the small intestine (pylorus), and then, once the tumor is located and the surrounding tissue is examined, the tumor is removed (Changazi *et al.*, 2020).

After the tumor is removed, the remaining parts of the pancreas, the bile duct, and the small intestine are reconnected. This procedure is considered a major surgery and it has a relatively high complication rate, and recovery time can be longer compared to other procedures.

2.5 Medication types

To relieve the symptoms caused by AHH in patients, there are two medication types that may be administered to patients. In this section, these medication types are introduced to familiarize the reader.

2.5.1 Diazoxide

Diazoxide's primary mechanism of action is to inhibit insulin release from the beta cells of the pancreas, thereby increasing blood glucose levels. Diazoxide works by opening potassium channels in the beta cells of the pancreas. This action hyperpolarizes the cell membranes, which prevents calcium influx, an essential step in insulin secretion. As a result, the drug reduces insulin secretion and raises blood sugar levels (Hansen, 2006).

The drug can be administered orally or intravenously. While it is generally well-tolerated, it can lead to several side effects such as fluid retention, hyperuricemia (excess uric acid in the blood), and hyperglycemia (excess glucose in the blood, the opposite of hypoglycemia) (Chen *et al.*, 2021). The reference medication for patients with an insulinoma is diazoxide, but it is not effective in all patients, and can lead to several adverse effects.

2.5.2 Octreotide

For patients who do not react well to diazoxide, octreotide is an alternative medication (Goode *et al.*, 1986).
Octreotide mimics the action of the hormone somatostatin, inhibiting the release of a variety of other hormones, including insulin, glucagon, and growth hormone from the pancreas. It is this property that makes it useful in the management of insulinoma. By inhibiting insulin secretion, octreotide helps to regulate and stabilize blood glucose levels in patients with this condition (Vezzosi *et al.*, 2005).

The drug is usually administered via subcutaneous injection, though it can also be given intravenously (Vezzosi *et al.*, 2005). Side effects can include gastrointestinal issues such as diarrhea and stomach cramping. However, these side effects are typically manageable and do not outweigh the benefits for most patients (Katz *et al.*, 1989).

2.6 Polyclinic visits

As part of the diagnostic pathway, a patient attends a follow-up visit at the polyclinic about a week after undergoing an imaging procedure to discuss the results. If the imaging reveals the presence of an insulinoma, the patient will then have a consultation with a surgeon scheduled. During this meeting, they will explore the possibility of surgery and discuss its potential risks and benefits. This approach aligns with the clinical practice in the Netherlands, as outlined by dr. Hans Hofland.

3. Research question and methodology

In this chapter the research question is presented, after which the different methods used to answer the research question are discussed and explained.

3.1 Research question

This report attempts to answer the following research question:

Is a diagnostic pathway containing the ^{68}Ga-NODAGA-exendin-4 PET/CT imaging technique cost-effective for localizing insulinomas compared to current imaging technique standards in the Netherlands? If so, what is the most cost-effective combination and order of imaging techniques for a diagnostic pathway in the Netherlands?

3.2 Literature research

Literature research was performed on insulinomas, conventional and experimental imaging techniques concerning insulinoma localization and surgery types. The results of this research are illustrated in sections 2.1 to 2.4.

3.3 Interviews

Several interviews with experts in the field of neuroendocrine tumors and insulinomas were conducted to receive input on modeling choices and assumptions. Interviews with experts in the field helped to fill knowledge gaps where insufficient insight could be retrieved from available literature. Expert interviews were used to construct the conventional and experimental diagnostic pathways used for this analysis, as presented in sections 4.1.1 and 4.1.2.

3.4 Cost-effectiveness analysis

3.4.1 Cost and effects

For this specific cost-effectiveness analysis, the cost embodies the monetary costs a patient incurs from the moment the patient is diagnosed with AHH and enters the diagnostic pathway to localize a potential insulinoma, until the patient leaves the diagnostic pathway due to the insulinoma being localized or due to there not being an insulinoma. The cost covered in this analysis are the cost of imaging techniques, pre-operative medication, polyclinic visits and surgery.

The effect is expressed in terms of quality-adjusted life-years (QALYs) allocated to a patient during his/her time in the diagnostic pathway. The QALY aims to combine the two most significant aspects of a health intervention, being its impact on quality of life of a patient and its impact on survival as assessed in terms of life years, into a single statistic (Gray *et al.*, 2010). A single QALY equates to a life year lived in perfect health.

For a patient in this model, the QALYs are then calculated as follows. The number of days a patient with an insulinoma spends in the model pre-operatively are multiplied with the average pre-operative quality of life (QoL). The number of days the patient spends in the model post-operation are multiplied with the post-operative QoL. Adding these two together results in the QALYs allocated to that patient during the time spent in the model.

3.4.2 ICER calculation and relevance

In a cost-effectiveness analysis, we first determine the costs and effects of a particular intervention and one or more alternatives, then we determine the differences in costs and effects, and lastly we present these differences as a ratio, or the price per unit of impact or result on health (Weinstein *et al.*, 1977).

Frequently used terms are the incremental costs, incremental effects, and the incremental cost-effectiveness ratio (ICER), since the emphasis is on the differences between two (or more) choices for different treatments or diagnostic pathways. Most of the time, the two choices represent an experimental new option on the one hand and the current commonly accepted standard on the other. If there are two alternatives, **A** being an experimental diagnostic pathway and **B** being a conventional diagnostic pathway (for example), we first determine the costs and effects of each, we determine the difference between the costs and effects, and finally we determine the ICER, which is the result of dividing the cost difference between A and B by the difference in effect between A and B:

$$\text{ICER} = \frac{\text{Cost}_{\text{A}} - \text{Cost}_{\text{B}}}{\text{Effect}_{\text{A}} - \text{Effect}_{\text{B}}} = \frac{\Delta\ \text{Cost}}{\Delta\ \text{Effect}}$$

Equation 1: formula for ICER

In this specific cost-effectiveness analysis, we rely on a simulation model to determine the cost-effectiveness. In this model, incremental costs and effects are determined every iteration of the model to calculate the ICER. An ICER scatter plot can then be used to plot the incremental costs and effects for the different iterations and to see whether the resulting ICERs indicate a cost-effective healthcare intervention. This is done by comparing the ICERs to the WTP threshold which is accepted in the relevant healthcare setting. The WTP threshold is the monetary amount society is willing to pay for added health benefit, in this case a QALY, for people with a certain medical condition. If the ICER is below the accepted WTP threshold, then the experimental technology may be deemed cost-effective. Conversely, if the ICER is above the WTP threshold then the opposite holds. Figure 5 is used to further clarify the relationship between the ICER and the WTP threshold. The green line running diagonally from the bottom left to the top right is an example WTP threshold. If an ICER for an experimental healthcare intervention is somewhere in the plane below the WTP threshold, then it and may be deemed cost-effective when considering this particular WTP. If the ICER is above the WTP threshold in the plane, then the opposite holds.

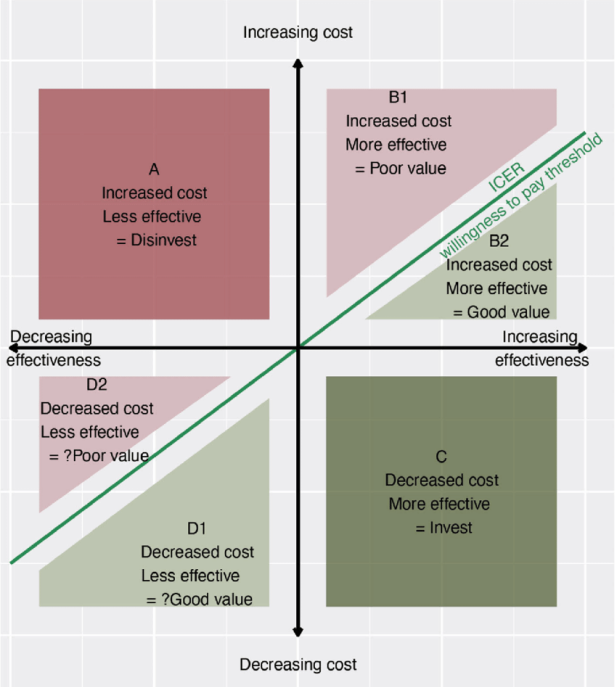

Figure 5: ICER cost-effectiveness plane (Graziadio et al., 2020)

The resulting ICER plot is provided in section 5.2.2 to indicate the incremental costs and effects model output of the different conventional and experimental diagnostic pathways.

3.4.3 NMB calculation and relevance

The NMB can be calculated by multiplying the QALYs per patient on average with the relevant WTP threshold and deducting from that result the cost of the intervention per patient.

$$\text{NMB} = \text{WTP} \times \text{QALYs} - \text{Cost}$$

Equation 2: formula for NMB (QALYs and Cost are average per patient)

The NMB thus shows whether the monetary value society has attached to the QALYs through the WTP threshold outweighs the monetary cost that is associated with these QALYs gained, meaning that a positive NMB indicates that a healthcare intervention is cost-effective (York Health Economics Consortium, 2016). Conversely, the diagnostic pathway with the highest NMB at a certain WTP threshold is the most cost-effective strategy. In the previous section, it was stated that the ICER can also be used to see whether an experimental healthcare intervention is cost-effective at a certain WTP. To see which experimental healthcare intervention is the most cost-effective and part of the 'frontier', the NMB is used.

The NMB is also used for the cost-effectiveness acceptability curve (CEAC). The CEAC determines the probability of each diagnostic pathway of being the most cost-effective at each separate WTP threshold, i.e. having the highest NMB. This probability across all WTP

thresholds is visualized using a line for each diagnostic pathway. Additionally, the CEAC determines the diagnostic pathway with the highest average NMB at each separate WTP threshold and adds a square shape to the line of that diagnostic pathway at that WTP, indicating it is considered the frontier. Note that this is fundamentally different from the diagnostic pathway with the highest probability of being the most cost-effective: the frontier is the strategy with the highest average NMB across all runs at that WTP threshold, but it could be that there is a strategy with a higher percentage of runs in which it was cost-effective at that WTP threshold.

The resulting CEAC plots are provided in section 5.2.3.

3.5 Discrete event simulation in R

Discrete event simulation (DES) is a modeling technique that is commonly used in health technology assessment (HTA) to understand and analyze the behavior of complex systems. In healthcare, DES is applied to model and quantify the performance of hospitals, healthcare networks and diagnostic pathways (Hajjarsaraei *et al.*, 2018). A DES model, like other simulations, is an imitation of the behavior of a real-world system over time (Landa *et al.*, 2018) and therefore has some advantages over performing a cost-effectiveness analysis in the real world with real patients.

With no practical or financial ramifications, a DES model can be used to pinpoint crucial areas and system bottlenecks, as well as provide quantitative answers to hypothetical what-if questions (Stahl *et al.*, 2003). This is a benefit of performing a DES simulation over doing real-world trials and exposing real patients to (experimental) procedures. Virtually no costs are incurred when using a DES model and vast amounts of (virtual) patients can be walked through the model, which for a rare disease like insulinomas would have taken centuries to accomplish otherwise. The development of a DES model of course requires a monetary investment, but this is often considerably less than performing actual trials.

For this particular instance, a DES model was chosen over a Markov model. A Markov model is another commonly used modeling approach in healthcare and represents a system as a set of states and transitions between those states, with the probability of transitioning from one state to another determined by the current state (Vázquez-Serrano *et al.*, 2021). A DES model is uniquely characterized by its approach to transitions, relying on event occurrence rather than state changes. Notably, it incorporates the time aspect in these transitions, emphasizing the occurrence of events over time, rather than at fixed intervals. This feature sets it apart considerably from other models like Markov. Therefore, since time to event data is available for this analysis, a DES model becomes a compelling choice, as it provides a more nuanced representation of time to event compared to the more static, discrete time approach of alternative models (Raphael *et al.*, 2017). For this reason, a DES model was chosen over a Markov model.

Events, entities, attributes and resources are the main concepts of a DES model. An event is anything that takes place in the environment at a certain moment in time. An example of an event in this particular DES model, is the outcome of an imaging technique. An imaging technique may or may not localize the insulinoma based on a probability and then send the

patient through to the next event. Entities are self-contained entities that have attributes and makes use of resources while encountering events in the context of healthcare. An example of an entity within a DES model is a patient, which is also the entity for this DES model (Cooper *et al.*, 2007; Ramwadhdoebe *et al.*, 2009). Attributes are features or characteristics that are exclusive to an entity and can change over time. Age and medical history are two examples of attributes that can be altered over time and affect an entity's path through the simulation, as well as the time intervals between events (Ramwadhdoebe *et al.*, 2009). Objects or facilities that provide a service to an entity are referred to as resources (Marshall *et al.*, 2015). Examples of resources in this DES model are CT scans, MRI scans and operating rooms.

For a more elaborate coverage of the model itself, including an example schematic diagram of the model, parameter calculations and the justification of assumptions made, see chapter 4.

4. Approach for calculating cost-effectiveness

In this chapter, the model description is provided, as well as the data used in the model and the assumptions made.

4.1 Model description

Through expert interviews, information on the conventional diagnostic pathway and potential experimental diagnostic pathways that use the Exendin imaging technique was retrieved. This information has allowed for the development of conventional and experimental diagnostic pathways, as presented in section 4.1.1 and section 4.1.2, respectively. To explain the implementation of the diagnostic pathways in the model, the schematics of one of the diagnostic pathways (the conventional diagnostic pathway) is shown and described in section 4.1.3. The schematics of all five diagnostic pathways are placed in Appendix II of this report.

4.1.1 Conventional diagnostic pathway

The conventional diagnostic pathway, making use of conventional imaging techniques, is the diagnostic pathway that patient currently go through in clinical practice. The experimental diagnostic pathways, making use of the Exendin imaging technique in addition to conventional imaging techniques. The experimental diagnostic pathways are described and motivated in section 4.1.2.

When it comes to the conventional diagnostic pathway, internationally speaking there is no single diagnostic pathway that physicians rely on. Treatment centers around Europe (including the ones involved in the previous research by Boss *et al.*, 2019) all have their own unique approach when diagnosing insulinoma patients. The difference between centers can be in terms of the sequence of e.g., the imaging techniques, but there can also be a difference in applied techniques altogether. For example, some centers may apply a technique called arterial stimulation venous sampling (ASVS) regularly for patients for whom non-invasive imaging techniques cannot localize the insulinoma, whereas other centers may not even apply ASVS at all.

The difficulty here is that for the simulation, there has to be a single reference conventional diagnostic pathway to which the experimental diagnostic pathways can be compared. Simulating all diagnostic pathways currently applied throughout Europe would be highly inefficient. However, the fact that there is no such thing as a common diagnostic pathway across European treatment centers, makes it difficult to say what a good conventional diagnostic pathway would then entail on a European level. Considering the fact that this analysis is performed at a Dutch university in the Dutch healthcare setting, it was decided during the expert interviews to opt for a conventional diagnostic pathway that matches with the most common Dutch practice. This means that the conventional diagnostic pathway includes the most commonly applied imaging techniques in the Netherlands, as well as the most common sequence in which they are applied in.

During expert interviews with dr. J. Hofland from the Erasmus MC and prof. dr. Martin Gotthardt and dr. Marti Boss from the Radboud UMC, the conventional diagnostic pathway was constructed. The experts indicated that the most common procedure was to start with the non-invasive imaging technique CT. If the insulinoma is not located, the patient undergoes an MRI scan. If the insulinoma is still not located, the invasive EUS technique is deployed. Finally, if the EUS also did not manage to locate the insulinoma, the patient undergoes the DOTA scan. Based on these expert insights, the conventional diagnostic pathway with the following sequence of imaging techniques was constructed: CT-MRI-EUS-DOTA.

4.1.2 Experimental diagnostic pathways

In accordance with expert opinion, it was decided to simulate five experimental diagnostic pathways. Each experimental diagnostic pathway will be the conventional diagnostic pathway CT-MRI-EUS-DOTA with Exendin inserted at different points. For example, the first experimental diagnostic pathway is Exendin-CT-MRI-EUS-DOTA, the second CT-Exendin-MRI-EUS-DOTA, etc.

Unfortunately, the dataset did not contain sufficient data to calculate the conditional probability for DOTA. DOTA would have been at the end of all experimental pathways due to its location in the conventional diagnostic pathway CT-MRI-EUS-DOTA. Because of this position near the end of the pathways, all patients in the dataset already had their insulinoma localized by the other imaging techniques that are performed earlier in the diagnostic pathways, leaving zero patients to determine the conditional probability of DOTA. Conditional probabilities and their role in the model are explained in section 4.2.2. It was therefore decided to remove DOTA from the experimental diagnostic pathways, resulting in four instead of five experimental diagnostic pathways. The four experimental diagnostic pathways are presented in table 2.

Table 2: names and sequences of techniques for experimental diagnostic pathways

Exendin+CT-MRI-EUS	**CT-MRI-Exendin-EUS**	**CT-Exendin-MRI-EUS**	**CT-MRI-EUS-Exendin**
Exendin + CT	CT	CT	CT
MRI	MRI	Exendin	MRI
EUS	Exendin	MRI	EUS
	EUS	EUS	Exendin

4.1.3 Schematic model representation

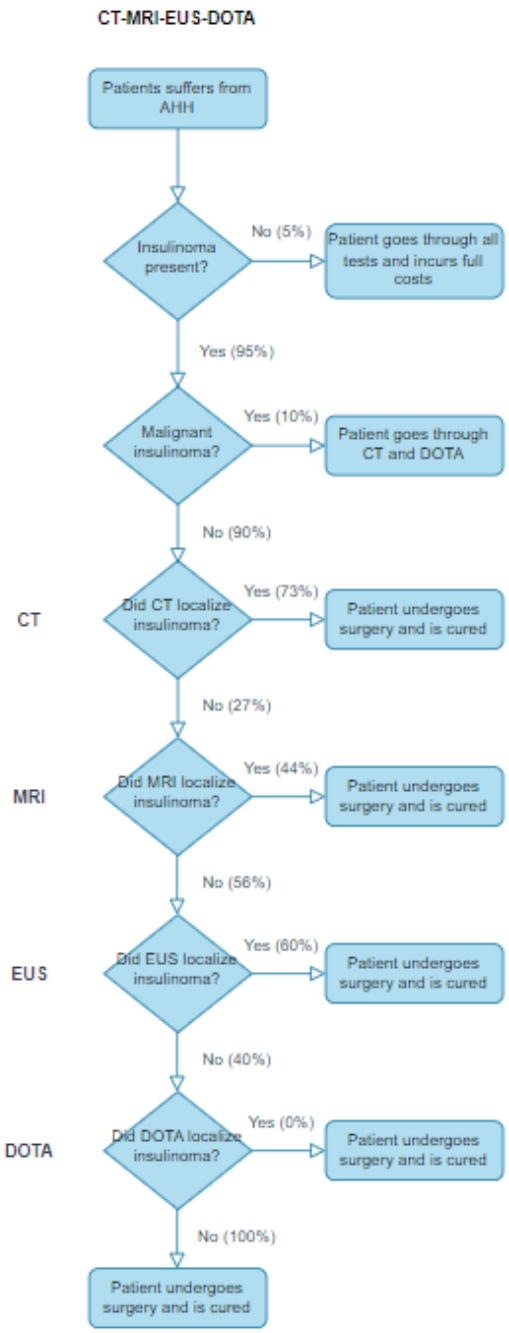

Figure 6: conventional diagnostic pathway

Before diving into the schematics and giving an example of the different steps involved in a diagnostic pathway, it is important to first explain the different icon types used in the schematics. In the schematics, there are three different types of icons: rectangles, rhombi and arrows. The rectangles simply give information about the virtual patient or indicate what the patient undergoes, for example stating that the patient is diagnosed with AHH or that the virtual patient undergoes surgery. The rhombi require a bit more explanation. Rhombi indicate a probability based event occurring, which works as follows. For every probability based event, a random number is drawn from a uniform distribution between 0 and 1 and is compared to the probability of the event having a *positive* outcome. What a *positive* outcome entails differs and is context dependent, but becomes clear from every event. An example of a *positive* outcome: a virtual patient undergoes an imaging technique, after which the imagine technique localizes the insulinoma. An example of a *negative* outcome: a virtual patient undergoes an imaging technique, after which the imagine technique does not localize the insulinoma. These probabilities are derived from literature, interviews or from the dataset provided by previous research performed by Boss *et al.*, 2019. If the random number is lower than the probability of a *positive* outcome, then the *positive* outcome is the outcome of the event. If the random number is higher than the probability, then the outcome of the event is the *negative* outcome. This way, a randomized path is generated for every patient in the model. Finally, the arrows simply indicate the flow of a patient through the model between the different rectangles and rhombi.

Now that the definitions of the different symbols in the schematics have been explained and illustrated, we can exemplify the further workings of a schematic by using one of the schematics as an example. Figure 6 shows the schematic of the conventional diagnostic pathway. The title of the diagnostic pathway refers to the imaging techniques present in the

diagnostic pathway and their respective order. To clarify: the distributions for the time the virtual patient spends before undergoing his first imaging technique, in between the imaging techniques and before undergoing surgery after having an insulinoma localized are not indicated in this schematic representation. The time and cost aspect are taking into consideration in the actual R model, but are left out in the schematics to simplify matters.

For illustrational purposes, let us say the virtual patient enters the conventional diagnostic pathway as presented in figure 6. The first square element which a virtual patient encounters already reveals the first assumption made in this model, namely that the virtual patients entering the care pathways all haven been previously diagnosed with AHH. After a virtual patient has been diagnosed with AHH, he/she encounters the first rhombus, indicating a probability based event in the model. The workings of a rhombus and a probability based event have been explained previously. In this first rhombus, it is determined whether the patient really has an insulinoma or not. Approximately 95% of patients suffering from AHH actually have an insulinoma, whereas the other 5% do not have an insulinoma, but do experience the symptoms and are thus going through the same diagnostic pathway. This is relevant, since the 5% who do not have an insulinoma do go through all imaging techniques in the diagnostic pathway. All this without ever having an insulinoma localized, but incurring all costs along the way. Therefore, this chance has to be taken into consideration for the model, as these patients do have an impact on the cost outcomes.

The first rhombus has two outgoing arrows, the right one corresponding to the 5% of virtual patients that do not have an insulinoma and the bottom one corresponding to the 95% of virtual patients who do have an insulinoma. The 5% without an insulinoma immediately encounter a rectangle, stating what are the consequences for this virtual patient. This rectangle forms the end station for these patients in this diagnostic pathway. The 95% who do have an insulinoma follow the bottom arrow and encounter their next rhombus, which determines whether the virtual patient has a malignant insulinoma.

Ten percent of patients have a malignant insulinoma. Expert input from dr. Hans Hofland helped shape this part of the model. It was decided to only take the diagnosis of malignant insulinoma into consideration and leave further treatment out of the diagnostic pathway, due to their more complex treatment. In case of a malignant insulinoma, the virtual patient follows the arrow to the right and enters a rectangle, indicating the virtual patient will leave the model after this. The virtual patient first enters the CT scan, after which enough evidence already points towards the possibility of a malignant insulinoma, and to confirm, a DOTA scan is performed. At this point, it has become clear that the virtual patient has a malignant insulinoma and he therefore leaves this diagnostic pathway. This assumption is discussed in section 4.3.2.

If the virtual patient is among the 90% of patients who do not have a malignant insulinoma, he/she continues to the CT scan. This is the first event related to an imaging technique, namely the CT scan. The CT scan could localize the insulinoma with a 73% probability (or not localize the insulinoma with a 27% probability). If the CT localizes the insulinoma for a patient, the patient leaves the rhombus through the arrow on the right to a rectangle. This rectangle states that the virtual patient undergoes surgery, is cured and leaves the

diagnostic pathway. In case the insulinoma is not localized by the CT scan, the virtual patient leaves the rhombus through the arrow on the bottom to another rhombus, namely the rhombus in which the virtual patient undergoes the MRI scan. The process for the virtual patient in this rhombus is exactly the same as it was in the previously covered rhombus for the CT scan, as there are again two outcomes for the virtual patient: the insulinoma is localized by the MRI and the virtual patient undergoes surgery, or the insulinoma is not localized and the virtual patient goes on to the next imaging technique. There is however a slight difference here regarding the calculation of these probabilities. This process is covered in the next section.

4.1.4 Conditional probabilities

The probabilities for the MRI and consecutive imaging techniques are so-called *conditional probabilities*. A conditional probability is the probability of an event, given the *condition* that another event has already occurred. In the case of the MRI, the *conditional probability* takes the event that the previous imaging technique CT did not localize the insulinoma into account.

For the remaining rhombi related to imaging techniques, the process of determining the next step for the virtual patients is all the same. They all rely on conditional probabilities to determine the next step for the virtual patient. The final rhombus, which in this diagnostic pathway is the DOTA method, is also the final point where a virtual patient may have his insulinoma localized. If the final method fails in localizing the insulinoma, the patient leaves the rhombus through the arrow on the bottom and does enter surgery. During this surgery, surgeons will rely on intraoperative palpation to localize the insulinoma, instead of preoperative localization.

4.1.5 Competing probabilities

Throughout the diagnostic pathways, there are events that depend on competing probabilities. These events determine the type of medication a patient may receive preoperatively and the type of surgery a patient may undergo. There are for example three options for medication and let us say that the chance of receiving medication 1 is called p1, the chance of receiving medication 2 is called p2 and the chance of receiving medication 3 is called p3. A patient can only receive one type of medication, so a construction was needed to select only one medication type per patient. The construction in figure 7 is a schematic representation of the construction that is used in the model for such events that have competing probabilities.

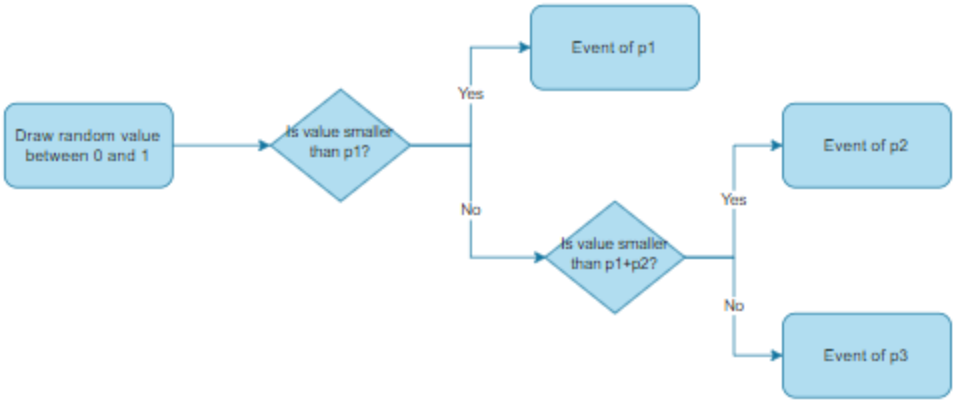

Figure 7: construction used for competing probabilities

Following the schematic from left to right: a random value is drawn between 0 and 1 using a random number generator. If the drawn value is lower than the probability of p1 in our medication example, then the arrow tagged yes is followed and the event of p1 is selected: the patient receives medication type 1. If the drawn value is higher than p1, the arrow tagged no is followed and the model checks whether the value is lower than p1+p2. If this holds, the arrow tagged yes is followed and the event of p2 is selected: the patient receives medication type 2. If the random value is higher than p1+p2, the arrow tagged no is followed and the event of p3 is selected: the patient receives medication type 3.

4.1.6 Number of patients

Using the simmer package in R, the model for the cost-effectiveness analysis is built and run. The number of patients per run was set to 5.000 patients. This number was chosen as it was found that patient numbers above 5.000 resulted in PC memory issues and rendered the model non-functional. In appendix IV the process of finding this number is further elaborated upon.

4.1.7 Relevant WTP threshold

In the Netherlands, the WTP threshold ranges from €20.000 to €80.000, depending on the proportional shortfall of the medical condition (Reckers-Droog *et al.*, 2018; Zorginstituut Nederland, 2015). The proportional shortfall is the ratio of health lost due to a medical condition to the total potential health going forwards. The proportional shortfall is determined as follows:

$$\text{Proportional shortfall} = \frac{\text{Remaining QALYs without condition} - \text{Remaining QALYs with condition}}{\text{Remaining QALYs without condition}}$$

Equation 2: formula for proportional shortfall

For this analysis, the time horizon is 2000 days, as is further motivated in section 4.1.8. The remaining QALYs without condition amount to 2000 days times the perfect QoL score per day. The remaining QALYs with condition amount to combined value of the average number of days spent by patients pre-operatively in the conventional diagnostic pathway times the

average pre-operative QoL score per day and the average number of days spent by patients post-operatively in the conventional diagnostic pathway times the average post-operative QoL score per day. The resulting proportional shortfall for AHH is 0,157. A paper by Zorginstituut Nederland, 2015 indicates that proportional shortfalls between 0,1-0,4 have a WTP threshold of €20.000 per QALY, so €20.000 per QALY is the relevant WTP threshold for this analysis.

4.1.8 Time horizon

The time horizon of the model was chosen after simulating 100,000 patients going through the model and determining the longest time a patient spent in the model pre-operatively afterwards. The time horizon of 2000 days strongly exceeds the longest pre-operative time. This is important, since otherwise the QALY scores of patients during this time horizon could be determined by the time-horizon being too short, instead of the time the model assigned to them in the pre-operative state.

4.1.9 QALY calculation

The question arises: in what way does implementing Exendin in a diagnostic pathway affect the health outcomes of patients? Exendin has a higher accuracy than the conventional imaging techniques, but how does this higher accuracy result in better or worse QoL for patients? Implementing Exendin in a diagnostic pathway will result in a shorter time a patient will spend pre-operatively, since Exendin has a higher accuracy than conventional imaging techniques and will therefore allow more patients to have their insulinoma(s) localized earlier, allowing them to also have surgery earlier. Less time spent in a pre-operative state is better for patients, since the post-operative QoL is on average higher than the preoperative QoL, due to the symptoms being mostly relieved after surgery. Simply put: the gain in QALY with Exendin is achieved by reducing time a patient spends in the pre-operative state and increasing the time spent in the post-operative state.

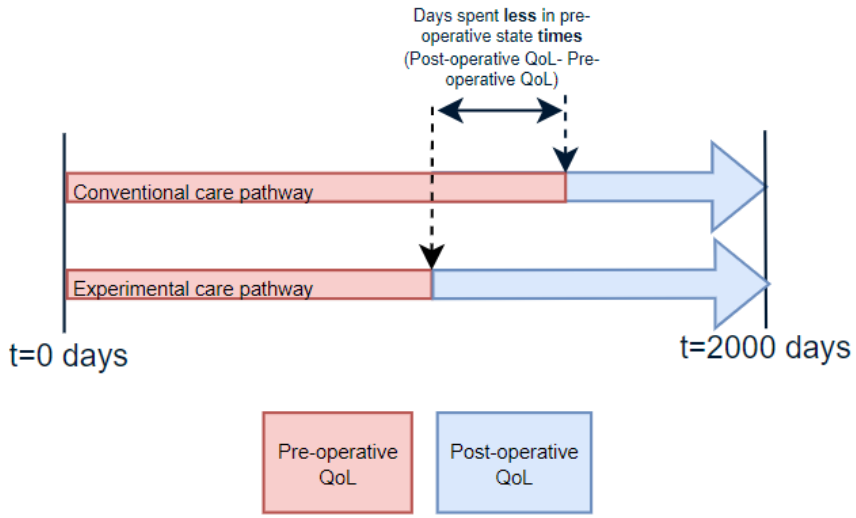

Figure 8: diagram showing QoL calculation for experimental diagnostic pathway, time goes from left to right. The dashed lines indicate the moment of surgeries for the experimental and conventional care pathways

Figure 8 shows the time gain for patients in the experimental diagnostic pathway: the red part of the arrow, indicating the pre-operative QoL, is shorter for the experimental care pathways due to the better accuracy of the Exendin and the often earlier surgery date for most patients, as explained earlier in this paragraph. The double-pointed arrow in the top-middle indicates the time gain for the experimental diagnostic pathway and is supported by the text right above, which provides the formula for the QALY gain as a consequence of this time gain.

The model, by drawing from the time distributions provided in section 4.2.2, determines the number of days a patient spends pre-operatively and multiplies this number with the QoL score it drew from the distribution for pre-operative QoL provided in section 4.2.1. This results in the pre-operative QALYs allocated to a patient. The model then deducts the number of pre-operative days of the patient from the time horizon of 2000 days and multiplies the resulting number with the QoL score it drew from the distribution for post-operative QoL provided in section 4.2.1. This results in the post-operative QALYs allocated to a patient.

4.2 Data for calculation

Regarding patient data and imaging techniques, predominantly the dataset on insulinoma patients from previous research by Boss *et al.*, 2019 was used in this cost-effectiveness analysis. Additionally, data found through literature research was used, as well as data gathered through expert interviews. Data on cost of e.g., medication, surgery and imaging techniques was mostly retrieved by consulting different departments of the Radboud UMC. In this section, the data on the quality of life, time distributions, costs and imaging techniques accuracies are given and described. Sources for all data will be given as well.

4.2.1 Data on quality of life distributions

During the research performed by Boss *et al.*, 2019, 59 patients with insulinomas were asked to fill in SF-36 QoL questionnaires (SF-36 is a standard for QoL questionnaires). These questionnaires were filled in twice: once before surgery and once 8 weeks after surgery, giving insight in the impact the surgery has on the QoL of patients. These SF-36 scores were converted into EQ-5D scores, which was necessary to use the scores in QALY related calculations. This conversion from SF-36 to EQ-5D was done using an algorithm developed by Freemantle *et al.*, 2013 and allows for individual patient level SF-36 QoL scores. In the model, the value of the pre-operative QoL is drawn from a beta distribution. The value of the post-operative QoL is then determined by drawing from a normal distribution fitted to the differences between the pre- and post-operative QoL scores in the patient data and adding the drawn value to the pre-operative QoL. The distributions for the QoL scores are given in table 3.

Table 3: distribution for QoL (based on survey results of 59 patients, as presented in Appendix I) (Boss et al., 2019)

QoL parameter	Value	95% CI	Parameters	Distribution	Source
Pre-operative QoL	0,727	0,533-0,884	a=16.736468, b=6.284288	beta	Boss *et al.*, 2019
Delta between pre- and post-operative QoL	0,132	0,092-0,172	mean=0,132, SE=0,0206	normal	Boss *et al.*, 2019

4.2.2 Data on time to event parameters

The duration of a patient's journey through the diagnostic pathway significantly impacts their health outcomes. The trial data from Boss *et al.*, 2019 provides a basis for understanding the time-to-event parameters. However, the mean values derived from this data significantly deviate from reference values for waiting times provided by dr. Hans Hofland, which are based on his clinical experience. As a result, a decision was made to conduct the analysis using two different time to event parameters: one using the trial data from Boss *et al.*, 2019, and one using dr. Hans Hofland's reference values. The time to event parameters based on the data from Boss *et al.*, 2019 and the reference values provided by dr. Hans Hofland are shown in table 4 below.

Table 4: distributions for waiting times based on trial data provided by Boss et al., 2019 and dr. Hans Hofland

Time to event parameter	Value	95% CI	Parameters	Distribution	Source	Value	Source
DaysBeforeMRI	**24,1**	15,237-33,049	mean= 24,14286 SE= 4,543873	normal	Boss *et al.*, 2019	**35**	dr. Hans Hofland
DaysBeforeDOTA	**11,4**	7,393-15,321	mean= 11,35714 SE= 2,02247	normal	Boss *et al.*, 2019	**35**	dr. Hans Hofland
DaysBeforeExendin	**15,8**	11,244-20,445	mean= 15,84444 SE= 2,347351	normal	Boss *et al.*, 2019	**35**	dr. Hans Hofland
DaysBeforeEUS	**16**	8,097-23,903	mean=16 SE= 4,032015	normal	Boss *et al.*, 2019	**28**	dr. Hans Hofland
DaysBeforeSurgery	**42,6**	35,587-49,697	mean= 42,64211 SE= 3,599677	normal	Boss *et al.*, 2019	**28**	dr. Hans Hofland

4.2.3 Data on costs

Since the main dataset on patient data stems from research by Boss *et al.*, 2019, which focused on multiple treatment centers from multiple countries, a decision had to be made regarding the origin of the costs used for the analysis. It would not be efficient (and possibly not even feasible) to perform the analysis using the costs of all the different centers. Availability of data would pose a significant problem, but it would also yield little added value. In section 4.1.1 it was stated that this analysis would be geared towards a conventional diagnostic pathway based on the most commonly applied Dutch variant. To then perform the analysis multiple times with costs from another country would say something about how these costs would affect the Dutch case, but would say little to nothing about the case in the other country, depending on how much the diagnostic pathway differs from the Dutch case. It was therefore decided to only use costs relevant for the Dutch setting: the costs of the different imaging techniques, the medication administered to patients, polyclinic visits and surgeries were all retrieved from price databases related to the Radboud UMC, a treatment center operating in the Dutch healthcare setting.

Considering the fact that this analysis is performed at the Radboud UMC in the Dutch healthcare setting, it was decided that the costs charged at the Radboud UMC were to be used as a reference. The outcomes of the analysis will still yield an indication of the cost-effectiveness of Exendin for treatment centers in the Netherlands, because of their similarities to the Radboud UMC. The costs of the different imaging techniques, the medication administered to patients, meetings with physicians during the diagnostic pathways and surgeries are given in table 5-8. All costs either originate from 2023 data or, if not, were corrected for the most recent 2023 price levels at the time of writing from the Dutch Central Statistical Office (CBS) (CBS, 2023). If prices in a table were corrected, it is indicated in the title of the table.

Table 5: costs of imaging techniques

Imaging technique	Costs	Source
^{68}Ga-DOTATOC	€1.765,60	Radboud UMC database
^{68}Ga-NODAGA-exendin-4 PET/CT	€1.765,60	Radboud UMC database
CT abdomen i.v. contrast	€527,47	Radboud UMC database
MRI abdomen i.v. contrast	€622,27	Radboud UMC database
EUS	€1000	Radboud UMC database

Table 6: costs of medication types

Medication	Costs (daily)	Source
Diazoxide	€1,5244	dr. Hans Hofland, Zorginstituut Nederland, 2023
Octreotide	€33,84	dr. Hans Hofland, Zorginstituut Nederland, 2023

Table 7: costs of polyclinic visits (corrected for 2023 price levels)

Polyclinic visits	Costs	Source
Visit for every imaging appointment	€197,96	Roijen *et al.*, 2015
Visit for surgery	€197,96	Roijen *et al.*, 2015

Table 8: cost of surgery types (corrected for 2023 price levels)

Surgery	Costs	Source
Whipple's procedure	€3.969	dr. Hans Hofland, Radboud UMC database, Patel *et al.*, 2022
Tail resection	€2.268	dr. Hans Hofland, Radboud UMC database, Patel *et al.*, 2022
Enucleation	€2.268	dr. Hans Hofland, Radboud UMC database Patel *et al.*, 2022

The costs for the imaging techniques were provided by the Financial Administration department of the Radboud UMC. The costs for the medication, polyclinic visits and surgery were calculated using data provided by the Financial Administration department of the Radboud UMC and the endocrinology department of the Erasmus UMC. The data provided by the endocrinology department of the Erasmus UMC included estimates of the use of medication of patients, the number of polyclinic visits a patient made and the average duration of the various surgery types.

The cost of medication was calculated using data from the Farmacotherapeutisch Kompas (Zorginstituut Nederland, 2023), a Dutch database of all Dutch registered and unregistered medication. It also includes data on the pricing of medication, so using this pricing, the cost of the medication used by patients could be calculated. Appendix III shows how these costs were calculated.

The costs of the polyclinic visits was found using data from the Dutch reference manual for economic evaluation in healthcare, which includes estimates for healthcare related costs (Roijen *et al.*, 2015). Using the estimated costs for a polyclinic visit of an academic hospital, the cost of a single polyclinic visit was retrieved. Based on input from dr. Hans Hofland, the model makes patients visit once for every imaging appointment and once before surgery.

The cost of the various surgery types was determined by multiplying the average duration of the relevant surgery types (in minutes) with an estimate of the cost of one minute of surgery. Estimates of surgery costs were used from a paper by Patel *et al.*, 2022. These costs do not specifically reflect the costs of the surgery types relevant for AHH as mentioned in section 2.4, since data on costs for these surgery types was unavailable at the time of writing. However, dr. Hans Hofland indicated that no specialized expensive tooling was required for the relevant surgery types, allowing this cost estimate for general surgery to be used.

4.2.4 Imaging technique conditional probabilities

Based on previous research performed by Boss *et al.*, 2019, the (conditional) probabilities of localizing the insulinoma for the different imaging techniques were determined. A more detailed explanation of conditional probabilities is provided in section 4.1.4 of this report. There are five combinations of conditional probabilities, one for every diagnostic pathway. The conditional probabilities are given in table 9-13 for the five different diagnostic pathways that were introduced in section 4.1.1 and section 4.1.2 of this report. In the column *Remaining/Located*, *Remaining* refers to the number of remaining patients who did not have their insulinoma localized by techniques earlier in the diagnostic pathway, if any. *Located* refers to the number of patients having their insulinoma localized by the imaging technique relevant for that row of the table.

Table 9: (conditional) probabilities for CT-MRI-EUS-DOTA, the conventional diagnostic pathway

Imaging technique	Value	95% CI	Parameters	Distribution	Remaining/Located	Source
CT	0,725	0,571-0,839	alpha=30, beta=12	beta	40/29	Boss *et al.*, 2019
MRI	0,444	0,187-0,738	alpha=5, beta=6	beta	9/4	Boss *et al.*, 2019
EUS	0,6	0,223-0,882	alpha=4, beta=3	beta	5/3	Boss *et al.*, 2019
DOTA	0	0,008-0,708	alpha=1, beta=3	beta	2/0	Boss *et al.*, 2019

Table 10: (conditional) probabilities for Exendin+CT-MRI-EUS diagnostic pathway

Imaging technique	Value	95 % CI	Parameters	Distribution	Remaining/Located	Source
Exendin + CT	0,981	0,901-0,995	alpha=53, beta=2	beta	53/52	Boss *et al.*, 2019
MRI	0	0,013-0,842	alpha=1, beta=2	beta	1/0	Boss *et al.*, 2019
EUS	1	0,158-0,987	alpha=2, beta=1	beta	1/1	Boss *et al.*, 2019

Table 11: (conditional) probabilities for CT-MRI-Exendin-EUS diagnostic pathway

Imaging technique	Value	95% CI	Parameters	Distribution	Remaining/Located	Source
CT	0,725	0,571-0,839	alpha=30, beta=12	beta	40/29	Boss *et al.*, 2019
MRI	0,444	0,187-0,738	alpha=5, beta=6	beta	9/4	Boss *et al.*, 2019
Exendin	0,8	0,359-0,957	alpha=5, beta=2	beta	5/4	Boss *et al.*, 2019
EUS	1	0,158-0,987	alpha=2, beta=1	beta	1/1	Boss *et al.*, 2019

Table 12: (conditional) probabilities for CT-Exendin-MRI-EUS diagnostic pathway

Imaging technique	Value	95% CI	Parameters	Distribution	Remaining/Located	Source
CT	0,725	0,571-0,839	alpha=30, beta=12	beta	40/29	Boss *et al.*, 2019
Exendin	0,909	0,615-0,979	alpha=2, beta=11	beta	11/10	Boss *et al.*, 2019
MRI	0	0,013-0,842	alpha=1, beta=2	beta	1/0	Boss *et al.*, 2019
EUS	1	0,158-0,987	alpha=2, beta=1	beta	1/1	Boss *et al.*, 2019

Table 13: (conditional) probabilities for CT-MRI-EUS-Exendin diagnostic pathway

Imaging technique	Value	95% CI	Parameters	Distribution	Remaining/Located	Source
CT	0,725	0,571-0,839	alpha=30, beta=12	beta	40/29	Boss *et al.*, 2019
MRI	0,444	0,187-0,738	alpha=5, beta=6	beta	9/4	Boss *et al.*, 2019
EUS	0,6	0,223-0,882	alpha=4, beta=3	beta	5/3	Boss *et al.*, 2019
Exendin	1	0,292-0,992	alpha=3, beta=1	beta	2/2	Boss *et al.*, 2019

4.2.4 Surgery type probabilities

Dr. Hans Hofland provided the different surgery types used to remove insulinomas in the Netherlands, along with their probabilities. These surgery types and probabilities are displayed in the table 14 below:

Table 14: surgery types and their probabilities

Surgery type	Probability	Source
Whipple's procedure	0,05	dr. Hans Hofland
Tail resection	0,20	dr. Hans Hofland
Enucleation	0,75	dr. Hans Hofland

4.2.5 Medication types probabilities

Dr. Hans Hofland also provided the different medication types that patients receive preoperatively on a daily basis, along with their probabilities. These medication types and probabilities are displayed in table 15 below:

Table 15: medication types and their probabilities

Medication type	Probability	Source
Diazoxide	0,70	dr. Hans Hofland
Octreotide	0,20	dr. Hans Hofland
(No medication)	0,10	dr. Hans Hofland

4.3 Assumptions

When building a model, making assumptions is inevitable. The model relies on the data that is provided, and the data is of course aggregated under certain conditions. These conditions have to be taken into account for the model, for which the assumption has to be made that these conditions also hold for the setting of the model. Acknowledging these conditions in the form of assumptions and being transparent is essential, as the relevancy for future use of the outcomes of the analysis is strongly determined by the assumptions made. Certain assumptions could make the outcomes of the analysis totally unapplicable to specific scenarios. The assumptions made for this model are therefore stated below, as well as their motivation.

4.3.1 Data assumptions

1. Patient specific properties such as gender and age are irrelevant for the treatment outcome of a patient. Due to a lack of data and literature on insulinoma, it is not possible to reliably correct for age and gender in patients. This assumption was validated by prof. dr. Martin Gotthardt and dr. Hans Hofland.

2. The cost of treatment is based on four factors: the cost of the imaging techniques, medication, polyclinic visits and (potentially) surgery. The patient might make additional costs due to adverse events or other causes, but due to a lack of literature on insulinomas, it was decided to simplify the model and focus on these four costs. Prof. dr. Martin Gotthardt and dr. Hans Hofland indicated that these are the relevant costs to focus on.

3. The postoperative QoL is the same for patients who underwent surgery after having the insulinoma localized via Exendin and for patients who underwent surgery after having the insulinoma localized via any other imaging technique. Prof. dr. Martin Gotthardt and dr. Hans Hofland indicated that this is a valid assumption to make.

4. The time to event parameters data, as documented by Boss *et al.*, 2019 and discussed in section 4.2.2, underwent truncation based on estimates for maximum waiting times derived from real-world waiting times for patients. Dr. Hans Hofland, drawing on his clinical experience, provided these estimates. The purpose of truncating the dataset was to ensure a more realistic representation of real-world waiting times. The values of the estimates of the maximum waiting times are provided in the table below:

Table 16: maximum waiting times used for truncation as provided by dr. Hans Hofland

Time to event parameter	**Maximum waiting time in days**
CT	28
MRI	60
DOTA	50
Exendin	50
EUS	48
Surgery	90

4.3.2 Modeling assumptions

1. Patients all have proven AHH (adult endogenous hyperinsulinemic hypoglycemia), as determined through a positive prolonged fasting test. This assumption was made, since in the real world only patients with proven AHH enter this diagnostic pathway. It is therefore fitting that the model also takes this into consideration.

2. Patients do not die while in the diagnostic pathway. The matter of patients dying while in the diagnostic pathway was discussed with prof. dr. Martin Gotthardt and he indicated that the death of patients is highly unlikely. Of course, patient death is always a possibility and can also be due to causes unrelated, but to simplify the model it was decided to leave the possibility of patient death out of the model.

3. There is only one conventional diagnostic pathway variant. This assumption was made to simplify the model, since in reality each treatment center has his own standard diagnostic pathway for AHH patients. Correcting for all these variations in the model, including the different possible experimental variants which would follow, would unreasonably enlarge the scope of the analysis. So although patients in real life will follow a diagnostic pathway that is unique to their respective treatment center, the virtual patients in the model will follow conventional (and corresponding experimental) diagnostic pathways based on the Dutch healthcare setting. This assumption was also already discussed in section 4.1.1.

4. The duration of the symptoms before diagnosis with AHH is not relevant for the treatment outcome of the patient. A similar reasoning preceded this assumption: due to a lack of data and literature, no reliable correction for symptom duration could be applied. This assumption was validated by prof. dr. Martin Gotthardt and dr. Hans Hofland.

5. A shorter time between diagnosis and surgery does not yield a better treatment outcome (or a higher quality of life after surgery). The same reasoning a with the previous two assumptions led to this assumption. Prof. dr. Martin Gotthardt indicated that this was a valid assumption to make.

6. Patients with malignant insulinoma leave the diagnostic pathway after diagnosis. This decision was made to simplify the model and keep the scope of the analysis within realistic bounds. This decision was supported by dr. Hans Hofland and prof. dr. Martin Gotthardt.

7. Patients whose insulinoma is not localized through any of the imaging techniques undergo surgery within the same waiting period as patients whose insulinoma is localized by the final imaging technique in the diagnostic pathway. During this surgery, surgeons will rely on intraoperative palpation to localize the insulinoma, instead of preoperative localization through an imaging technique. In reality, patients who have an insulinoma will at one point in time undergo this type of surgery, but the time until this surgery can vary between patients. For some patients, it could be clear that they have an insulinoma, in which case they will undergo surgery relatively quickly. In other cases, the

presence of an insulinoma might not be so evident, resulting in patients having to wait for surgery longer. Because of the lack of data regarding the time until surgery for patients with an insulinoma who did not have their insulinoma localized, it was decided to allocate a time between the final imaging technique in the diagnostic pathway and surgery identical to that of patients with an insulinoma who did have their insulinoma localized by the final imaging technique. This assumption was validated by prof. dr. Martin Gotthardt and dr. Hans Hofland.

5. Model outcomes and health economic impact

In section 5.1, the numerical cost-effectiveness outcomes of a PSA are presented. A visual representation of these outcomes is presented in section 5.2, using cost-effectiveness plots, incremental cost-incremental effectiveness plots and a cost-effectiveness acceptability curve (CEAC). In section 5.3, the health economic implications of the results are reflected upon. In section 5.4, a one-way sensitivity analysis (OWSA) of the PSA results is performed. In section 5.5, a OWSA of the DSA results is performed.

5.1 Cost-effectiveness outcomes (PSA)

After simulating all five diagnostic pathways for 1.500 runs with 5.000 patients per run through a PSA, the cost-effectiveness results were obtained. The simulation was performed using both the waiting times provided by research by Boss *et al.*, 2019 and the estimates provided by dr. Hans Hofland. The average cost per patient and the average QALY per patient are given per diagnostic pathway for both waiting time sources in table 17-18.

The incremental cost, incremental effect and ICER are also given in table 17-18. The CEAC in section 5.2.3 will further illustrate the WTP ranges for which strategies were most cost-effective.

Table 17: average cost, QALY per patient, incremental cost, incremental effect, ICER per strategy based on trial data provided by Boss et al., 2019

Strategy	Cost (€)	Effect (QALY)	Incremental Cost (€)	Incremental Effect (QALY)	ICER (€)	Compared to
CT-MRI-EUS-DOTA	5.078,85	4.674				
CT-MRI-Exendin-EUS	4.878,82	4.674	-200,03	0,00022	**-880.614,50**	CT-MRI-EUS-DOTA
CT-MRI-EUS-Exendin	4.983,61	4,674	-95,23	0,00009	**-1.079.199,00**	CT-MRI-EUS-DOTA
CT-Exendin-MRI-EUS	5030,66	4,676	151,83	0,00153	**99.161,14**	CT-MRI-Exendin-EUS
Exendin+CT-MRI-EUS	6380,05	4,677	1349,40	0.00176	**767.743,10**	CT-Exendin-MRI-EUS

Table 18: average cost, QALY per patient, incremental cost, incremental effect, ICER per strategy based on estimates by dr. Hans Hofland

Strategy	Cost (€)	Effect (QALY)	Incremental Cost (€)	Incremental Effect (QALY)	ICER (€)	Compared to
CT-MRI-EUS-DOTA	5.021,46	4,676				
CT-MRI-Exendin-EUS	4812,89	4,677	-208,59	0,00061	**-339.534,80**	CT-MRI-EUS-DOTA
CT-MRI-EUS-Exendin	4.913,66	4,677	-107,80	0,00061	**-175.693,10**	CT-MRI-EUS-DOTA
CT-Exendin-MRI-EUS	4.965,94	4,679	153,07	0,00151	**101.264,40**	CT-MRI-Exendin-EUS
Exendin+CT-MRI-EUS	6.270,93	4,682	1304,99	0,00378	**345.481,50**	CT-Exendin-MRI-EUS

In addition to the average cost and effect outcomes for each diagnostic pathway, the average number of days a patient spends in each diagnostic pathway is stated. As stated before in section 3.4.1, the number of days a patient spends in the diagnostic pathway in a pre-operative state determines the QALYs gained.

Table 19: average number of days in diagnostic pathway per diagnostic pathway based on trial data provided by Boss et al., 2019

Strategy	Average number of days in diagnostic pathway	Standard deviation
CT-MRI-EUS-DOTA	43,5	5,2
CT-MRI-EUS-Exendin	43,3	5,2
CT-MRI-Exendin-EUS	43,0	5,1
CT-Exendin-MRI-EUS	39,5	3,4
Exendin+CT-MRI-EUS	35,6	3,1

Table 20: average number of days in diagnostic pathway per diagnostic pathway based on estimates provided by dr. Hans Hofland

Strategy	Average number of days in diagnostic pathway	Standard deviation
CT-MRI-EUS-DOTA	37,5	4,1
CT-MRI-Exendin-EUS	36,1	3,7
CT-MRI-EUS-Exendin	36,1	3,7
CT-Exendin-MRI-EUS	32,7	2,8
Exendin+CT-MRI-EUS	24,2	1,1

5.2 Graphical cost-effectiveness outcomes simulation (PSA)

In this section, the cost-effectiveness plots, incremental cost-incremental effectiveness plots and CEAC are given, visualizing the numerical outcomes of the PSA provided in the previous section.

5.2.1 Cost-effectiveness plots

First, the Cost-Effectiveness plots are provided below in figure 9, for both waiting time sources. Note that Ex stands for Exendin in the legend on the right of the figure. The difference in cost between the Exendin+CT-MRI-EUS and other diagnostic pathways is evident. This makes sense, considering the fact that a large portion of patients in this diagnostic pathway will undergo the relatively expensive Exendin imaging technique together with the CT imaging technique, making it the most costly option.

To emphasize: the cost-effectiveness plot on the left, based on time to event estimates provided by dr. Hans Hofland, does not take parameter uncertainty into consideration. The plot on the right, based on time to event parameters relying on data provided by Boss *et al.*, 2019, does take parameter uncertainty into consideration.

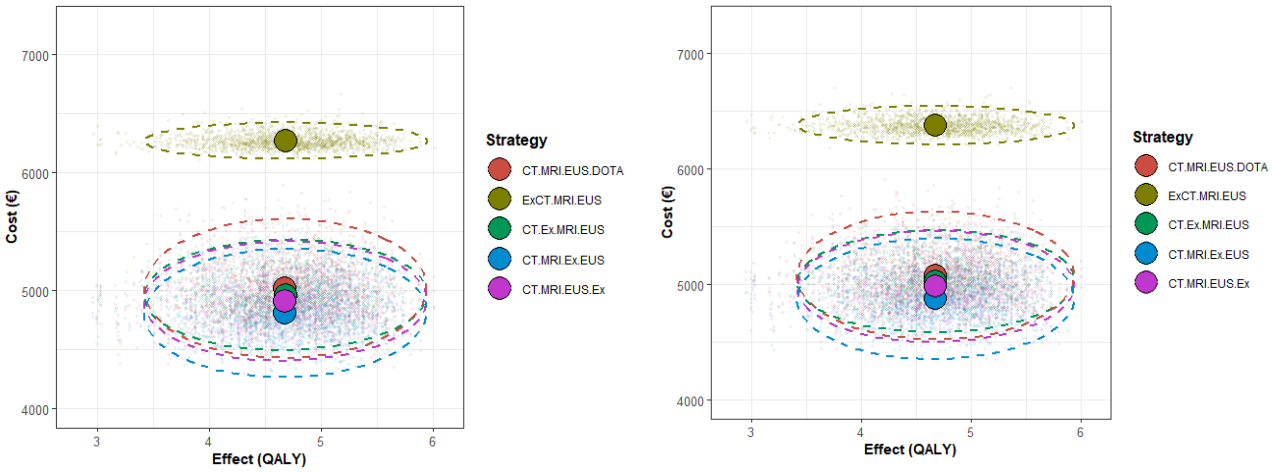

Figure 9: Cost-Effectiveness plots of PSA based on waiting time estimates by dr. Hans Hofland on the left, based on waiting times based on trial data provided by Boss et al., 2019 on the right

5.2.2 Incremental cost-incremental effectiveness plots

Below in figure 10, the incremental effectiveness and incremental cost as compared to the conventional diagnostic pathway CT-MRI-EUS-DOTA are plotted for the four *experimental* diagnostic pathways. The WTP lines for the upper and lower bound of the WTP range in the Netherlands are plotted as well. Note that Ex again stands for Exendin in the legend on the right.

From this plot, the location of the dots corresponding to the Exendin+CT-MRI-EUS diagnostic pathway already makes it clear it would be too expensive for a WTP of €20.000 and perhaps also a WTP of €80.000. The other three diagnostic pathways appear to have a better chance of being cost-effective, even for a WTP of €20.000.

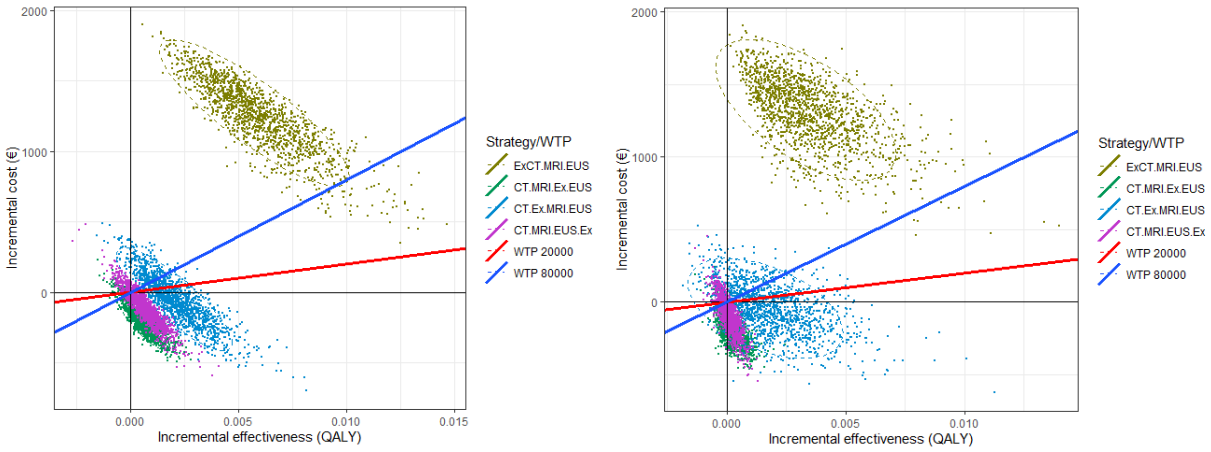

Figure 10: Incremental cost-incremental effectiveness plot of PSA based on waiting time estimates by dr. Hans Hofland on the left, based on waiting times based on trial data provided by Boss et al., 2019 on the right

5.2.3 CEACs

In figure 11 below, the CEACs of the PSA results are plotted for the different diagnostic pathway compositions. Note that Ex again stands for Exendin in the legend on the right.

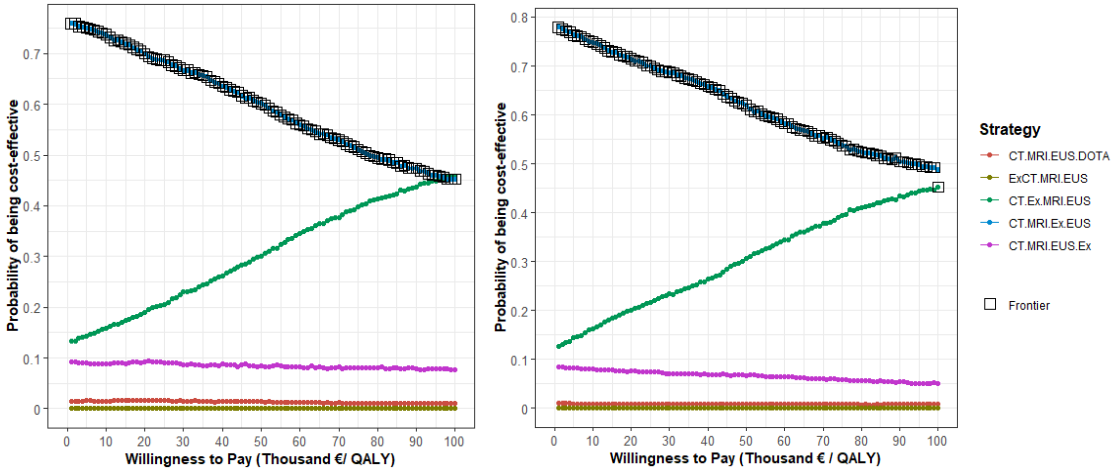

Figure 11: CEACs of PSA based on waiting time estimates by dr. Hans Hofland on the left, based on waiting times based on trial data provided by Boss et al., 2019 on the right

The CEACs are plotted for a WTP threshold range of €0-€100.000, but for the Dutch WTP threshold range of €20.000-€80.000, there is a single diagnostic pathway that is on the frontier for all WTP threshold values. For the PSA based on waiting times provided by dr. Hans Hofland and for the PSA based on trial data provided by Boss et al., 2019, the CT-MRI-Exendin-EUS diagnostic pathway is on the frontier.

Thus, for the relevant WTP threshold in the Netherlands of €20.000, as was motivated in section 4.1.7, the CT-MRI-Exendin-EUS diagnostic pathway is on the frontier in both CEACs.

5.3 Health economic implications of simulation outcomes

The outcomes of the PSA show that the conventional diagnostic pathway CT-MRI-EUS-DOTA is never on the frontier in the CEAC plots in section 5.2.3. Note that there still is a chance of this pathway being the most cost-effective, but the model predicts that there are other diagnostic pathways with a greater probability of being the most cost-effective at every WTP threshold in the CEAC plot.

As was stated earlier in section 4.1.7 of this report, the relevant WTP threshold for AHH in the Netherlands is €20.000, meaning that Dutch society is willing to pay €20.000 for a QALY gained for patients with AHH. This means that the diagnostic pathway with the highest average NMB at a WTP of €20.000 is the most cost-effective diagnostic pathway.

In the CEAC plots in section 5.2.3, the strategy with the highest average NMB at each separate WTP level is indicated as being on the frontier. This means that the diagnostic pathway which is on the frontier at WTP €20.000 is the most cost-effective diagnostic pathway. It is clear from the CEACs that the CT-MRI-Exendin-EUS diagnostic pathway is on

the frontier at this WTP, indicating that the CT-MRI-Exendin-EUS is the most cost-effective diagnostic pathway.

5.4 One-way sensitivity analysis (PSA)

From the PSA results, a OWSA was performed. This OWSA can be used to determine the impact of the model parameters on the outcomes of the results, in this case the NMB, but it can also be used to determine whether the model behavior is logical. In figure 12 below, the OWSA outcomes of the CT-MRI-EUS-DOTA diagnostic pathway are visualized using a tornado plot. The tornado plot shows whether parameter values that were above or below the mean value of the parameter in question (indicated by the fill color corresponding to "Parameter Level High/Low") led to high or low model outcome values in terms of NMB. The mean values of the different parameters can be found in section 4.2.

The OWSA was only performed for the PSA based on time to event parameter estimates provided by dr. Hans Hofland, due to the model structures being identical between both time to event parameter variants and performing the OWSA for both would not yield any additional insight into model behavior. The WTP threshold used for the tornado plot is €20.000, while the conventional NMB for the CT-MRI-EUS-DOTA diagnostic pathway is €88.727,90 at this WTP threshold for the OWSA based on waiting time estimates by dr. Hans Hofland.

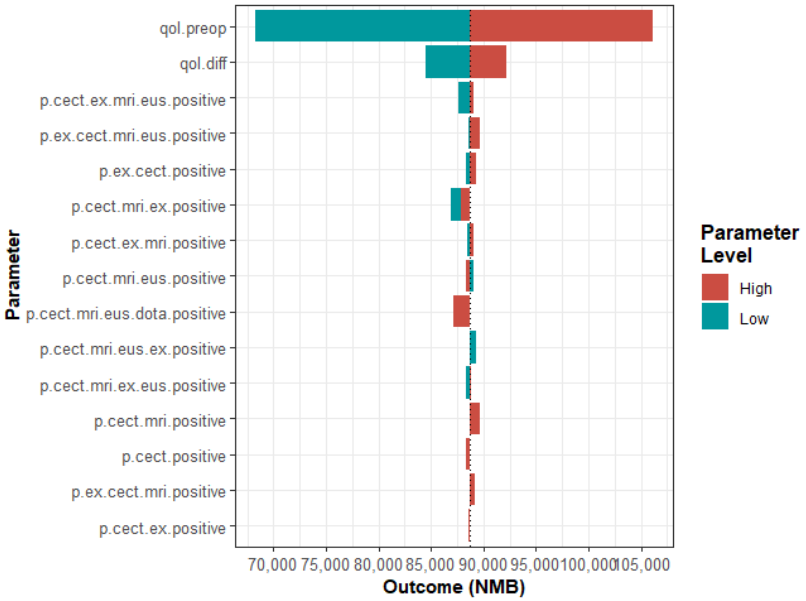

Figure 12: Tornado plot of the impact all model parameters on the NMB outcome of the CT-MRI-EUS-DOTA diagnostic pathway. OWSA based on time to event parameter estimates by dr. Hans Hofland

What stands out, is the large impact the parameter for the pre-operative QoL has on the outcomes of the model (qol.preop). Compared to the impact of other parameters, the impact is considerable. This impact is caused by the direct effect it has on the QALYs allocated to all patients in the diagnostic pathway, contrary to most other parameters which only affect a smaller percentage of patients. This direct effect on all patients, combined with the large 95% CI of 0,533-0,884 for the parameter, explains the large impact on the model.

From the tornado plot, it becomes clear that the behavior of the model is logical. High parameter values for the QoL scores lead to higher model outcomes, whereas low parameter values lead to lower model outcomes. For the parameters related to the accuracies of the imaging techniques, like the parameter for the accuracy of the CT scan (p.cect.positive), the same holds. Higher accuracies lead to higher model outcomes, which is sound, as higher accuracies lead to a shorter time spent pre-operatively. Lower accuracies lead to lower model outcomes, which is also indicative of logical model behavior, as lower accuracies lead to a longer time spent pre-operatively. This procedure of visually checking the tornado plots for logical model behavior was performed for all diagnostic pathways.

The tornado plots of all diagnostic pathways are provided in Appendix V and further illustrate that the behavior of the model in response to various parameter values is in fact logical.

5.5 One-way sensitivity analysis (DSA) for Internal Model Validation

In addition to a OWSA PSA, a OWSA DSA was performed to perform Internal Model Validation. The OWSA DSA was performed for all parameters with a sample rate of 100 per parameter range and 10.000 patients per sample. The parameters were all varied across a value range from 0 to 1. Using the OWSA DSA outcomes, it can again be checked whether the model shows logical behavior based on the various parameter input values. In addition, it can be shown how changing the value of a parameter can impact which diagnostic pathway is found to be the most cost-effective.

The OWSA DSA was again only performed for the DSA based on time to event parameter estimates provided by dr. Hans Hofland, due to the model structures being identical between both time to event parameter variants and performing the OWSA for both would not yield any additional insight into model behavior.

The outcome of the OWSA is plotted for every diagnostic pathway for four randomly selected parameters to illustrate whether or not the model shows logical behavior based on the various parameter values. The four plots are shown in figure 13.

From the outcomes of the OWSA of the p.cect.positive parameter, indicating the accuracy of the CT imaging technique, it becomes clear that the model behaves as expected when the value of the parameter increases. On the y-axis, the NMB is plotted. As the value of the parameter increases, the NMBs for the four diagnostic pathways which incorporate the p.cect.positive parameter in the model increase. This makes sense, as a higher accuracy of the imaging technique leads to a shorter time spent pre-operatively. The NMB of the Exendin+CT-MRI-EUS diagnostic pathway is not affected by the value of the parameter, which is sound since this diagnostic pathway does not incorporate said parameter.

The outcomes of the p.ex.cect.positive parameter, indicating the combined accuracy of the Exendin and CT imaging techniques, also show sound model behavior. Increasing the accuracy leads to a higher model outcome, due to a lower time spent pre-operatively. This parameter only affects the Exendin+CT-MRI-EUS diagnostic pathway in the plot, which is due to the parameter only being used in this diagnostic pathway. The outcomes of the qol.preop

parameter, indicating the value of the pre-operative QoL, are also logical. An increasing value of this parameter leads to higher model outcomes for all diagnostic pathways, which is again correct model behavior. Finally, the outcomes of the parameter p.cect.mri.positive, indicating the conditional accuracy of the MRI imaging technique after the CT imaging technique was performed, also exhibit coherent model behavior. An increasing accuracy leads to higher model outcomes, but only for the diagnostic pathways that incorporate this parameter. This procedure of visually checking the OWSA outcomes for logical model behavior was performed for all parameters.

The OWSA DSA outcomes for all parameters are provided in Appendix VI.

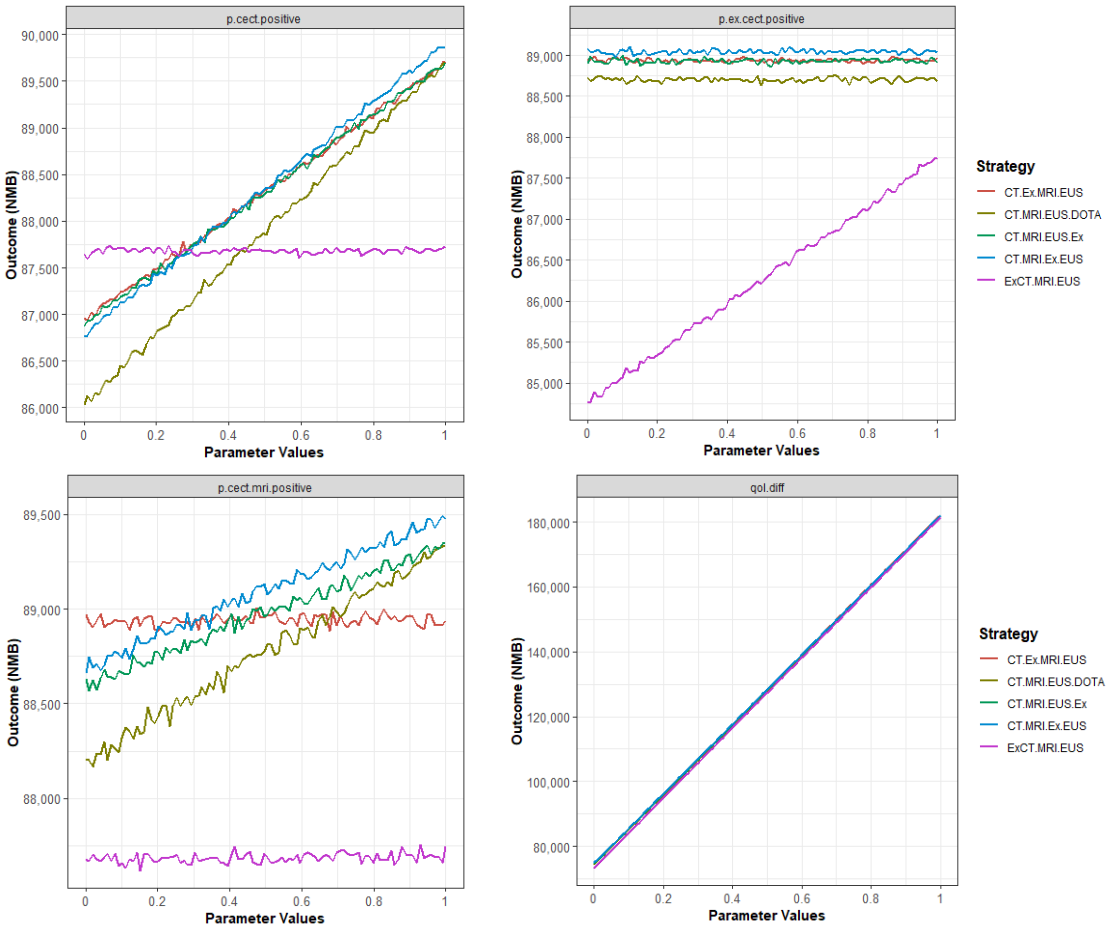

Figure 13: OWSA DSA outcomes for (clockwise, starting top left) p.cect.positive, p.ex.cect.positive, qol.diff and p.cect.mri.positive. OWSA based on time to event parameter estimates by dr. Hans Hofland

To show how changing the value of a parameter impacts which diagnostic pathway is found to be the most cost-effective, using the relevant WTP threshold of €20.000 and a parameter value range of 0-1, the most cost-effective diagnostic pathways were found across the parameter ranges. The most cost-effective diagnostic pathways across the parameter ranges are shown below in figure 14.

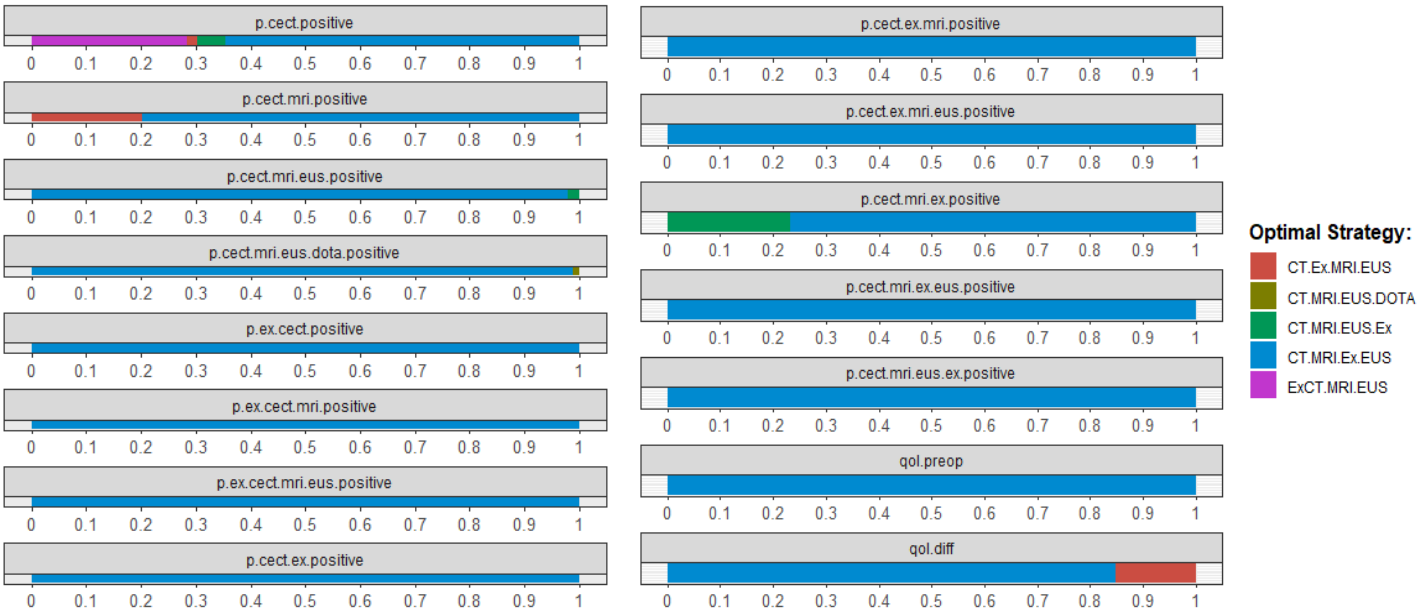

Figure 14: OWSA DSA output showing most cost-effective diagnostic pathway across parameter ranges. OWSA based on time to event parameter estimates by dr. Hans Hofland

Upon reviewing the average values of various parameters given in section 4.2 and figure 14, it's evident that slight variations in these averages do not significantly impact the results produced by the current model. There is no instance where the mean value of any model parameter approaches a critical point that would trigger a shift towards a different more cost-effective diagnostic pathway.

The figure also demonstrates that the model is sensitive to changes in the values of several parameters. A closer look at the parameter p.cect.mri.positive, for example, indicates that if the mean parameter value is decreased from the 44% provided by Boss et al., 2019, to 20% or lower, it causes a shift in the most cost-effective diagnostic pathway from CT-MRI-Exendin-EUS to CT-Exendin-MRI-EUS. This adjustment is justifiable, as a decrease in MRI accuracy would eventually suggest that incorporating Exendin earlier in the diagnostic pathway would yield a more cost-effective option. This logical pattern can also be seen when applying the same reasoning to all other parameters, reinforcing the model's rational behavior.

5.6 Resource usage

In response to rising medical expenses, there has been a growing focus on resource utilization within healthcare environments. As a result, the utilization of various imaging techniques was closely monitored, and the findings are presented in the following table.

Table 21: usage of different imaging techniques for percentages of patients across the diagnostic pathways, based on PSA using time to event parameter estimates by dr. Hans Hofland

Diagnostic pathway	Exendin scan (% of patients)	CT scan (% of patients)	MRI scan (% of patients)	EUS (% of patients)	DOTA scan (% of patients)
CT-MRI-EUS-DOTA		100%	33.1%	22.5%	28.4%
Exendin+CT-MRI-EUS	100%	100%	12.9%	12.0%	
CT-Exendin-MRI-EUS	33.3%	100%	13.6%	12.3%	
CT-MRI-Exendin-EUS	22.7%	100%	33.2%	13.7%	
CT-MRI-EUS-Exendin	15.4%	100%	33.1%	22.6%	

Between the current standard diagnostic pathway CT-MRI-EUS-DOTA and the pathway CT-MRI-Exendin-EUS, which was estimated to be the most cost-effective, the differences in resource usage are as follows. The pathway CT-MRI-Exendin-EUS does not use the DOTA scan, but instead relies on the Exendin scan. The Exendin scan is used in the CT-MRI-Exendin-EUS pathway for a smaller percentage of patients than the DOTA scan is used in the CT-MRI-EUS-DOTA pathway (22.7% and 28.4%, respectively). Since both the DOTA scan and the Exendin scan use the CT medical device to create the imaging itself, the use of the CT medical device is likely to decrease with the CT-MRI-Exendin-EUS pathway. In addition, EUS is applied less frequently in the CT-MRI-Exendin-EUS pathway compared to the CT-MRI-EUS-DOTA pathway (13.7% and 22.5%, respectively). This would imply that the CT-MRI-Exendin-EUS pathway would result in less of a burden for the capacity currently required for performing the EUS procedures.

5.7 Percentage of patients with non-localized insulinoma

The number of patients with an insulinoma who did not have their insulinoma localized in the different diagnostic pathways was tracked in the model. The resulting numbers are provided in the table below.

Table 22: percentage of patients with non-localized insulinoma, based on PSA using time to event parameter estimates by dr. Hans Hofland

Diagnostic pathway	Patients with non-localized insulinoma (%)
CT-MRI-EUS-DOTA	3.96%
Exendin+CT-MRI-EUS	0.66%
CT-Exendin-MRI-EUS	0.81%
CT-MRI-Exendin-EUS	1.21%
CT-MRI-EUS-Exendin	1.28%

6. Discussion

This cost-effectiveness analysis was performed to determine if a diagnostic pathway for patients with AHH incorporating Exendin would be a cost-effective alternative to the Dutch conventional diagnostic pathway, CT-MRI-EUS-DOTA. In the analysis, CT-MRI-EUS-DOTA, consisting of conventional imaging techniques, was compared to four experimental diagnostic pathways. These experimental diagnostic pathways were adaptations of the conventional diagnostic pathway, with Exendin at different time points. This resulted in four experimental diagnostic pathways: Exendin+CT-MRI-EUS, CT-Exendin-MRI-EUS, CT-MRI-Exendin-EUS and CT-MRI-EUS-Exendin. The experimental diagnostic pathway CT-MRI-Exendin-EUS was found to have the highest average NMB at the relevant WTP threshold of €20.000/QALY at €88.601. The conventional diagnostic pathway, CT-MRI-EUS-DOTA, had an average NMB of €88.396. Comparing CT-MRI-Exendin-EUS to the conventional diagnostic pathway, the incremental costs were -€200 and the QALYs were unaffected. The next best alternative diagnostic pathway CT-Exendin-MRI-EUS had an average NMB of €88.480. Comparing CT-Exendin-MRI-EUS to CT-MRI-Exendin-EUS, the incremental costs were €152 and the QALYs were unaffected. The diagnostic pathway CT-MRI-Exendin-EUS was thus estimated the most cost-effective in this analysis, due to it having the highest average NMB at the relevant WTP.

No similar research has been performed on the most cost-effective diagnostic pathway for AHH patients, therefore it is not possible to compare the outcomes of this research with other studies. In addition, no cost-effectiveness analyses on Exendin have been performed regarding this specific application, meaning that reflecting on how the results of this study align with prior research is not feasible.

A few remarks should be made regarding the limitations of this analysis. As stated in section 4.1.1 of the report, in order to simplify the model and reduce its scope, the decision was made to focus on a conventional diagnostic pathway which was based on the standard of care in the Netherlands. With insulinomas being a very rare condition with a yearly incidence of 1-4 people per million (Okabayashi *et al.*, 2013; Placzkowski *et al.*, 2009; Richards *et al.*, 2002), country specific literature on the topic is limited. Review papers analyzing the localization and treatment options, like a review by Mehrabi *et al.*, 2014, give some indication of current standards but lack the specificity required when considering a single country. A direct consequence of this, is that the model had to heavily rely on assumptions which were based on expert opinion. Although expert opinion is the best alternative to go by in such a scenario, it results in rough estimates entering the equation, which are not directly based on data but rely on intuition instead. However, due to time constraints, collecting real world data to replace these assumptions was not feasible within the scope of this analysis. The impact of such estimates on the final outcomes of the model can of course not be quantified at this point in time.

An additional note should be made about the decision to opt for a conventional diagnostic pathway based on the standard of care in the Netherlands. In section 4.1.1 of the report, said decision was made and motivated, and in section 4.1.2 the experimental diagnostic pathways are given and motivated. These experimental diagnostic pathways are effectively variants of the conventional diagnostic pathway, with the Exendin imaging technique

integrated at different places. This puts a heavy emphasis on the Dutch standard of care for this report, but this does not imply that the diagnostic pathway presented as the most cost-effective is in fact the best arrangement possible in general for a diagnostic pathway for AHH patients. There could in fact be a different arrangement of imaging techniques which would result in a higher cost-effectiveness, but not all possible arrangements were evaluated due to this report focusing solely on the Dutch setting, due to it providing the least obstacles in adoption given the context of the report. It could thus be that the most cost-effective diagnostic pathway variant possible was not found in this analysis, but the odds of this are slim due to the years of clinical experience in a well-developed healthcare system that have helped shape the current standard of care diagnostic pathway.

It was decided not to take malignant insulinoma into account for the remainder of the care pathway after the model has diagnosed the insulinoma as malignant, due to their more complex treatment. This assumption is also provided and validated through expert opinion in section 4.3.2. This assumption does have its consequences for the applicability of the modeling outcomes to the real world, since in the real world 10% of patients unfortunately do have a malignant insulinoma. In section 4.1.2, it is explained that the dataset on imaging technique accuracies provided by Boss *et al.*, 2019 does not contain enough data for a conditional probability of DOTA in the various *experimental* diagnostic pathways and that therefore, DOTA was left out of these pathways in the model. This is problematic for malignant insulinomas, since these show well on DOTA imaging, as experts indicated. We were unable to implement the DOTA scan in the model and could thus not consider malignant insulinomas in a realistic way. If it would have been possible to implement DOTA using a conditional probability and identify the malignant insulinoma through the DOTA, then the most cost-effective variant of the diagnostic pathway could have turned out differently because of the impact the DOTA scan had in its relevance for malignant insulinoma. If this analysis would be extended in the future, incorporating the DOTA into the experimental diagnostic pathways should be a priority and thus making sure sufficient data on every imaging technique accuracy is available, to also allow DOTA to be incorporated into the experimental diagnostic pathways.

Another assumption made in the modeling process, is that patients who enter a diagnostic pathway with an insulinoma and do not have their insulinoma localized through an imaging technique, receive surgery after undergoing the final imaging technique and do so after the same waiting period as patients who did actually have their insulinoma localized by the final imaging technique. This assumption is also provided and validated through expert opinion in section 4.3.2 and it was made because of a lack of data concerning the time before surgery for this group of patients. In the real world, patients who do not have their insulinoma localized do not receive surgery as fast as patients who did have it localized. Patients who do not have it localized often first go through a process of lifestyle changes to reduce the symptoms caused by the AHH. When these lifestyle changes appear to have no effect after a certain while, a potential insulinoma is again considered and the patient may undergo some imaging techniques again. It could then be the case that the insulinoma is localized, after which the patient finally receives surgery. The waiting time for surgery of a real-world patient who did not have it localized can therefore be much longer than the waiting time the model adopted because of said assumption. The consequences of this assumption for the applicability of the model outcomes to the real world could be significant, considering the

potential time gain for these patients could be hundreds of days spent less in a pre-operative state if Exendin manages to localize the insulinoma. As provided in section 5.7, it was found that 3.96% of patients in the conventional CT-MRI-EUS-DOTA pathway had an insulinoma which was not localized in the pathway. The diagnostic pathway CT-MRI-Exendin-EUS, which the model estimated to be the most cost-effective, yielded a percentage of 1.21%. These differences in percentages could result in considerable differences in reduced time in pre-operative state when comparing it to the average time gain the *experimental* diagnostic pathways now provided for regular patients in the model. It would therefore also be a recommendation to better account for patients who do not have their insulinoma localized, for which a better insight into the time before surgery for this group of patients.

A technical limitation of this analysis are the relatively low number of simulations runs and patients used for the simulations, due to high memory usage of the health economic model. Despite these computational limitations, it's important to note that the impact on the overall findings is likely minimal. Both versions of the model pointed to a distinct most cost-effective diagnostic pathway, even with the lower number of runs and smaller patient sample. While simulations with more runs and patients could potentially have offered more nuanced insights, we believe the cost-effectiveness outcomes would not have differed. However, a future extension of this analysis should aim to address these memory usage issues for more extensive simulations and remove this limitation.

For the performance of the different imaging techniques, the model relies on data provided by research performed by Boss *et al.*, 2019. The same thus holds for the CT, which is used in every diagnostic pathway explored in this analysis. Prof. dr. Martin Gotthardt indicated that the output of the CT was often examined in conjunction with the output of the DOTA. If for example the CT indicated that there was an insulinoma present, then this presumption would have led physicians to also see the insulinoma on the DOTA output more easily, or the other way around. This then results in cross-contamination between the performance of both the CT and DOTA, possibly resulting in an artificially better performance for both imaging techniques. The impact of this on the cost-effectiveness outcomes of the model will have been the greatest through the CT, referring to its position being the first or second imaging technique patients encounter in all diagnostic pathways used in this report. This could have had its effect on the cost-effectiveness outcomes of this analysis. If the diagnostic performance of the CT imaging technique was in fact artificially boosted through cross-contamination by the DOTA and the diagnostic performance of the DOTA was artificially boosted through cross-contamination the other way around, then this will have led to both the CT and the DOTA overperforming in the model. When considering modeling outcomes, this will have resulted in a conventional diagnostic pathway localizing more insulinoma at an earlier stage due to the CT scan overperforming, resulting in more QALYs allocated to patients. The DOTA will not have had an impact on the modeling outcomes, due to it being the final imaging technique patients encounter and the assumption made that the time before surgery is the same for patients with an insulinoma who did have it localized and for patients who did not have it localized. For the experimental diagnostic pathways, an overperforming CT will likely have resulted in a lower conditional probability for the Exendin scan, due to the CT scan having localized more insulinomas in the dataset than it did. This will result in experimental diagnostic pathways gaining less from having the Exendin scan integrated in the pathway, compared to the situation in which the CT scan was not boosted

and the Exendin scan had a higher conditional probability. Additionally, having the Exendin integrated at an earlier point in the diagnostic pathway will be less beneficial, due to the decreased relative diagnostic performance of the Exendin because of its lower conditional probability. Ultimately, the artificially boosted CT will lead to a smaller difference in QALYs allocated to a patient between the conventional and experimental diagnostic pathways, thereby reducing the potential benefits of applying the Exendin imaging technique. In addition, due to the lower conditional probability of Exendin, an *experimental* diagnostic pathway with Exendin integrated at an earlier point in the pathway will also have achieved a smaller relative difference in QALYs compared to what that same pathway would have done had the CT not been overperforming.

Initially, for time to event parameters the model only relied on data provided by Boss *et al.*, 2019, who worked with an international patient group during their research. Because of this international nature, patients experienced very different waiting times because of the differences in standard care practices between the respective countries. For the modeling and fitting of distributions, clinical limits provided by experts were taken into consideration to homogenize the dataset as much as possible, but comparing the resulting mean waiting times to reference values based on the Dutch clinical practice provided by dr. Hans Hofland showed that there was a significant difference. Tables 19 and 20 show the small differences in the number of pre-operative days between diagnostic pathways and clearly indicate the large impact that the waiting times have on the cost-effectiveness outcomes of the model. Every additional day in the diagnostic pathway counts in this model, since the model in essence only focusses on reducing pre-operative time. Another caveat of only relying on the dataset provided by Boss *et al.*, 2019, was the fact that some imaging techniques applied to localize insulinoma in the real world simply were performed earlier for most patients than other imaging techniques. This led to unrealistically long waiting times between the different imaging techniques themselves: waiting times between common practice CT and trial Exendin will be longer in the dataset, because of the common practice imaging technique CT having been performed earlier than trial Exendin, resulting in longer waiting times between these two techniques than between, for example, common practices CT and MRI. In reality, the waiting time for an imaging technique will of course be similar, no matter the prior performed imaging technique. The combined difficulty of the data not being based on a single standard of care and the data being unreliable due to real world interference necessitated the use of other data to determine the extent to which relying solely on the data from Boss *et al.*, 2019 was affecting the cost-effectiveness outcomes. It was decided to opt for estimates on waiting times in the Dutch healthcare setting from dr. Hans Hofland in addition to the original data provided by Boss *et al.*, 2019. This resulted in data that was representative for the relevant Dutch standard of care, making it a good fit for this analysis. The provided figures being estimates and not based on trial data is a drawback, but the positives of having relevant and comparatively reliable data were deemed to outweigh the negatives in this regard. Both the data from Boss *et al.*, 2019 and the estimates from dr. Hans Hofland resulted in the same diagnostic pathway being estimated to be the most cost-effective. Having the model indicate the same diagnostic pathway to be the most cost-effective, even when using different time to event parameters, indicates the robustness of the model. Different cost-effectiveness outcomes between different time to event parameters would have indicated a high sensitivity to time to event parameters and a high uncertainty around the cost-effectiveness outcomes, rendering the results of this research

largely inconclusive. We can now be fairly certain about this diagnostic pathway in fact being the most cost-effective, of course taking modelling limitations into consideration. A sidenote to make, is that for the reference data we were only able to retrieve insight from one expert on the Dutch clinical practice regarding waiting times due to time and resource constraints. A more ideal scenario would be to contact experts from more treatment centers and obtain multiple estimates of the Dutch clinical practice. Potentially, different waiting times could have been found and used as input, resulting in different cost-effectiveness outcomes.

This cost-effectiveness analysis heavily relies on the QoL data collected during the clinical trial performed by Boss *et al.*, 2019. Patients that underwent surgery to have their insulinoma removed filled in two questionnaires: one questionnaire pre-operatively and one questionnaire post-operatively. Without this insight in the QoL of patients, this cost-effectiveness analysis in its current form would not have been possible, as it was now able to take QoL scores of actual patients with an insulinoma into consideration. There is however still potential room for improvement regarding the QoL data. One could imagine that surgeons who could pre-operatively rely on the superior Exendin scan were able to perform the surgeries better than when they would not have had access to this technology. Expert opinion on the matter indicated that for this analysis, it was a valid assumption to make that this was not the case as it is hard to say how much benefit operating based on an Exendin scan would yield, but the fact remains that there could be a difference. It is unfortunately not possible to account for this potential Exendin-related QoL gain. Since all patients who underwent surgery and filled in the questionnaires underwent Exendin, meaning no patients underwent surgery without having undergone Exendin prior to surgery, meaning no post-operative differentiation was possible between patients who did undergo Exendin and patients who did not undergo Exendin. This limited the cost-effectiveness analysis to a time-horizon which only went until 2000 days, since simulating beyond this point did not have extra added value due to the QoL scores being identical beyond this point. Having a longer time horizon could have had its effects on the cost-effectiveness outcomes of the analysis, if the post-surgery QoL was in fact different for insulinomas located through Exendin. The often decades of time post-surgery have a much larger potential to accrue QALYs than the mere difference of days spent with a different QoL score in the current model. This means a higher post-operative QoL score would result in much more potential QALYs gained by diagnostic pathways that incorporate Exendin. If post-surgery QoL for insulinomas located through Exendin was higher, then the cost-effectiveness outcomes would have leaned towards an early implementation of Exendin more than they currently would have.

This cost-effectiveness analysis is aimed at finding the most cost-effective diagnostic pathway for patients with AHH and potentially an insulinoma and is not aimed at optimizing the time a patient waits before entering the diagnostic pathway. However, the data aggregated by Boss *et al.*, 2019 also includes data on symptom time, which represents the time patients had symptoms for, before undergoing their first imaging technique. Symptom times of 10 years and upwards were noted regularly. Of course, implementing the most cost-effective diagnostic pathway is very important, especially with the challenge of increasing cost of healthcare we are facing. Even so, the average difference in QALYs per patient between the most cost-effective diagnostic pathway and the conventional diagnostic pathway is 0,004 QALYs, or 1 days. Comparing these gains in effectiveness to the years some patients spend with a serious loss in QoL due to their symptoms, makes these gains almost

negligible. Instead, focusing on getting patients with AHH to enter the specialized diagnostic pathway as quickly as possible would hypothetically yield a far greater QoL gain. This is of course a difficult task considering the rarity of the condition, but perhaps more of the focus should be on this part of the issue, because of the potential for QoL gain. Such an approach may very well prove to be cost-effective, since people being ill and unable to contribute to society also cost money. A possible recommendation could be to increase awareness amongst GPs about AHH in general, to have patients referred to a specialized treatment center earlier. This way, the number of extreme cases of patients having to wait for over a year could potentially be reduced.

7. Conclusion

This cost-effectiveness analysis on ^{68}Ga-NODAGA-exendin-4 PET/CT aimed to answer the following research question:

Is a diagnostic pathway containing the ^{68}Ga-NODAGA-exendin-4 PET/CT imaging technique cost-effective for localizing insulinomas compared to current imaging technique standards in the Netherlands? If so, what is the most cost-effective combination and order of imaging techniques for a diagnostic pathway in the Netherlands?

To the first part of the research question, a diagnostic pathway containing Exendin was in fact estimated to be cost-effective. To the second part of the research question, the answer is that the CT-MRI-Exendin-EUS diagnostic pathway was estimated to be the most cost-effective. This diagnostic pathway maximized the average NMB at the relevant WTP threshold per QALY gained for AHH patients in the Netherlands of €20.000.

Appendix I

Patient	Pre-operative QoL	Post-operative QoL	Patient	Pre-operative QoL	Post-operative QoL	Patient	Pre-operative QoL	Post-operative QoL
1	0,835184236	0,922039809	R31	0,796042969	0,903713281	UTU002	0,469858559	0,8383875
2	0,784598142	0,75366	R32	0,784598142	0,75366	UTU003	0,708323125	0,72226875
R04	0,817998281	0,828962188	R34	0,817998281	0,828962188	UTU005	0,703310156	0,766544531
R05	0,636203351	0,902007969	R37	0,636203351	0,902007969	UTU006	0,767276215	0,849070226
R06	0,667522656	0,947690382	R38	0,667522656	0,947690382	UTU007	0,683403906	0,7648275
R07	0,696153976	0,8728375	R39	0,696153976	0,8728375	UTU008	0,674829601	0,7332925
R08	0,63600125	0,903174688	R40	0,63600125	0,903174688			
R09	0,71211408	0,924261319	R41	0,71211408	0,924261319			
R10	0,626526944	0,930093194	R43	0,626526944	0,930093194			
R11	0,666707344	0,886674288	UMCG001	0,666707344	0,886674288			
R12	0,834418594	0,870865	UMCG002	0,834418594	0,870865			
R13	0,569355069	0,907161944	UMCG003	0,569355069	0,907161944			
R14	0,798591163	0,944006563	UMCG004	0,798591163	0,944006563			
R15	0,906679063	0,947690382	UMCG005	0,906679063	0,963255069			
R16	0,7144075	0,758241369	UMCG006	0,7144075	0,758241369			
R17	0,797090625	0,813669688	UMCG007	0,797090625	0,813669688			
R18	0,626720642	0,856998559	UMCG008	0,626720642	0,856998559			
R19	0,660992656	0,938328594	UPPS001	0,660992656	0,938328594			
R20	0,803896094	0,963255069	UPPS002	0,803896094	0,963255069			
R21	0,842815313	0,936613906	UPPS003	0,842815313	0,936613906			
R22	0,832938142	0,940395538	UPPS004	0,832938142	0,940395538			
R23	0,825433924	0,887467188	UPPS005	0,758540938	0,813729861			
R24	0,840445	0,900046997	UPPS006	0,696932344	0,705865156			
R25	0,630720226	0,894671563	UPPS007	0,840401215	0,66709908			
R28	0,7627	0,854747969	UPPS010	0,777626736	0,751325156			
R29	0,648974531	0,963255069	UTU001	0,683880781	0,817394531			

Appendix II

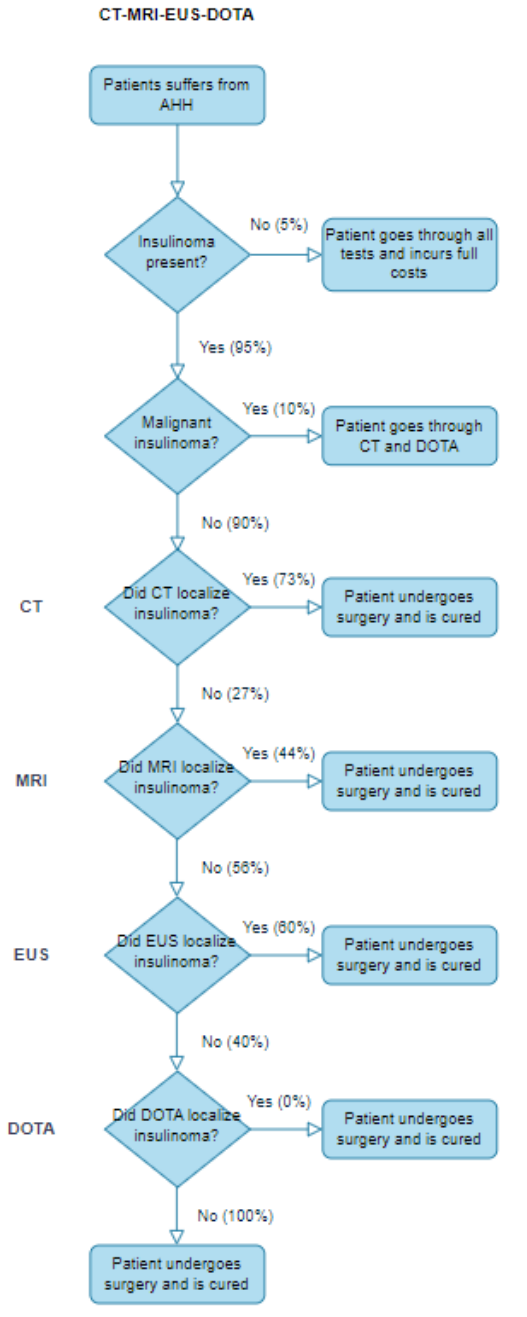

Figure 15: schematic representation of conventional diagnostic pathway CT-MRI-EUS-DOTA

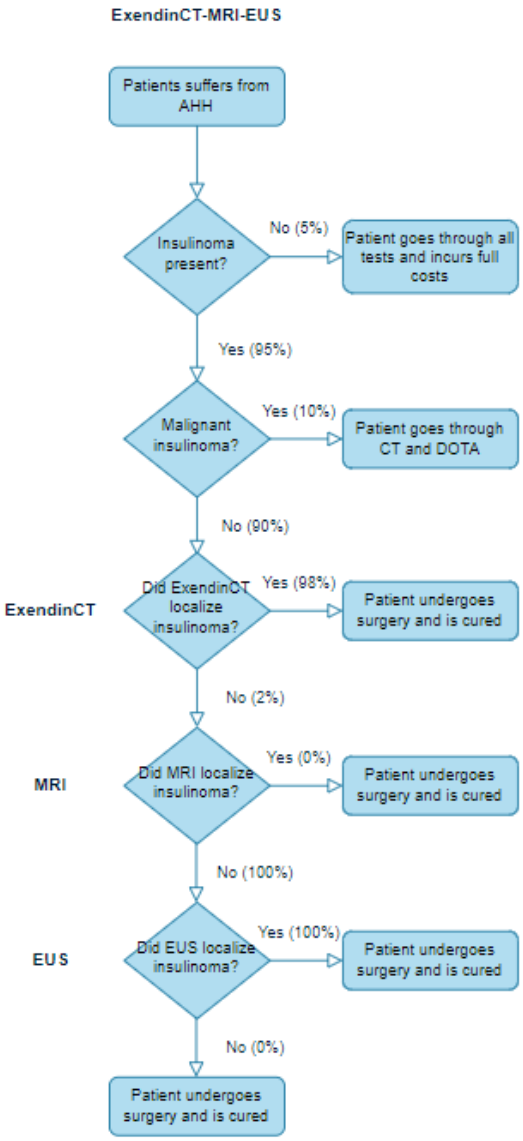

Figure 16: schematic representation of experimental *care path way ExendinCT-MRI-EUS*

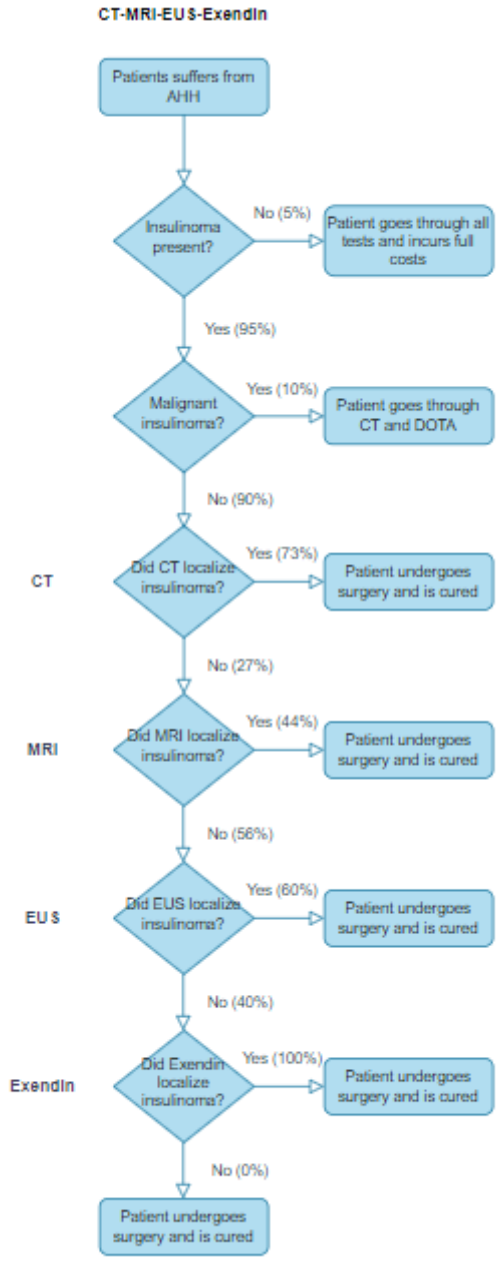

Figure 17: schematic representation of experimental diagnostic pathway CT-MRI-EUS-Exendin

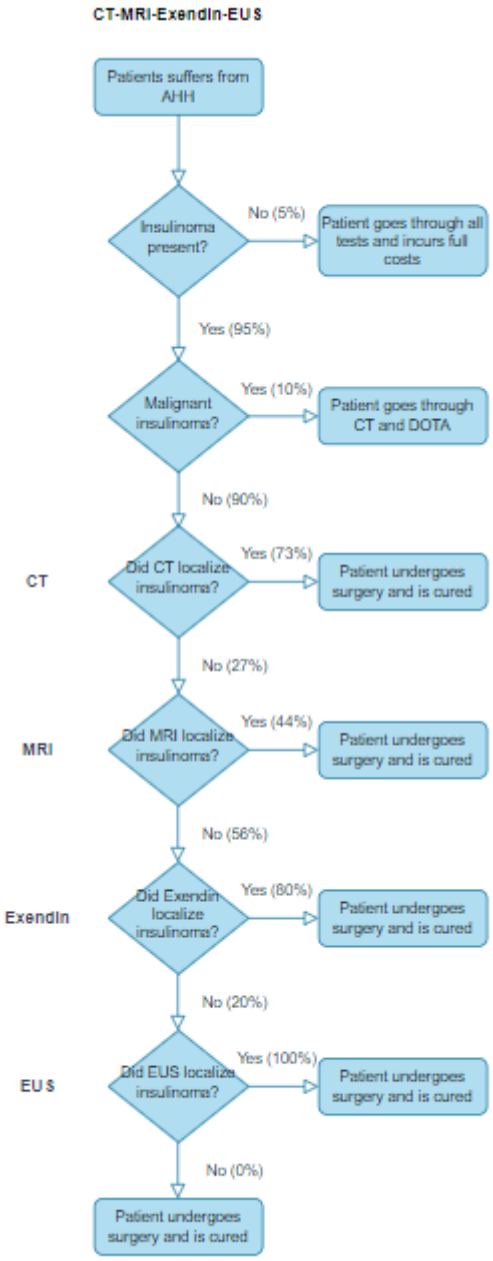

Figure 18: schematic representation of experimental *diagnostic pathway CT-MRI-Exendin-EUS*

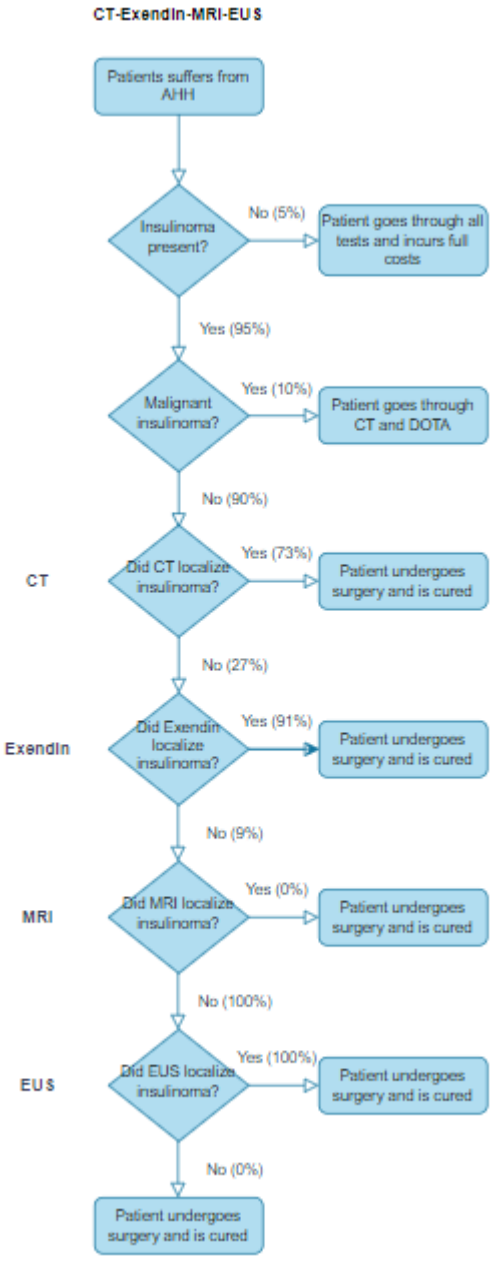

Figure 19: schematic representation of experimental *diagnostic pathway CT-Exendin-MRI-EUS*

Appendix III

The costs of the two medication types potentially consumed by patients pre-operatively are calculated in this appendix. Table 23 gives the daily dosages patients take of each medication type, as provided by dr. Hans Hofland. Table 24 shows the bulk purchasing costs for the medication types, as provided by the Farmacotherapeutisch Kompas.

Table 23: medication types and dosages

Medication type	**Dosage**	**Source**
Diazoxide	2x 100 mg daily	dr. Hans Hofland
Octreotide	3x 100 mcg daily	dr. Hans Hofland

Table 24: medication types and bulk purchasing costs

Medication type	**Bulk purchasing costs**	**Source**
Diazoxide	100x 100 mg = €76,22	Zorginstituut Nederland, 2023
Octreotide	50 mcg = €5,46	Zorginstituut Nederland, 2023

Using these values, the medication cost for both medication types can be calculated.

For **diazoxide**, the purchasing costs for 100 mg = €76,22/100 = €0,7622. Daily dosage costs are then: 2 * €0,7622 = €**1,5244**.

For Octreotide, the purchasing costs for 50 mcg = €5,46. Daily dosage costs are then:
6 * €5,46 = €**33,84**.

The resulting daily costs per medication type in table form:

Table 25: daily medication costs per patient per medication type

Medication	**Costs (daily)**	**Source**
Diazoxide	€1,5244	dr. Hans Hofland, Zorginstituut Nederland, 2023
Octreotide	€33,84	dr. Hans Hofland, Zorginstituut Nederland, 2023

Appendix IV

To identify the number of patients to simulate, a base case analysis (BCA) was performed. For the BCA, no parameter uncertainty was incorporated, but the stochastic uncertainty was. Using this BCA, the number of patients could be determined which was required to account for the impact of patient-level variation in the model outcomes. For this BCA, two diagnostic pathway strategies were used: the conventional diagnostic pathway CT-MRI-EUS-DOTA and the *experimental* diagnostic pathway ExendinCT-MRI-EUS. Five patient numbers were selected to check for performance (see table 26 for patient numbers) and for each patient number, both diagnostic pathways were simulated 100 times. The difference in cost between both diagnostic pathways was then calculated and the standard error of the mean (SEM) for this cost difference was determined per patient number. The SEM was then compared between patient numbers and the patient number at which the SEM started to level out was selected to keep the computational time within reasonable bounds. Additionally, boxplots were used, which show if the outcomes are symmetric, closely packed, and potentially skewed per patient number. These boxplots can be found in figure 20 below.

Due to PC memory issues arising during runs with 10.000 patients and up, it was decided to opt for 5.000 patients per run for the simulations to obtain the lowest SEM possible, given the technical challenges.

Table 26: number of patients and SEM

Number of patients simulated	**SEM (of difference in average cost per patient)**
1.000	12,96296
5.000	6,850664
10.000	4,703609

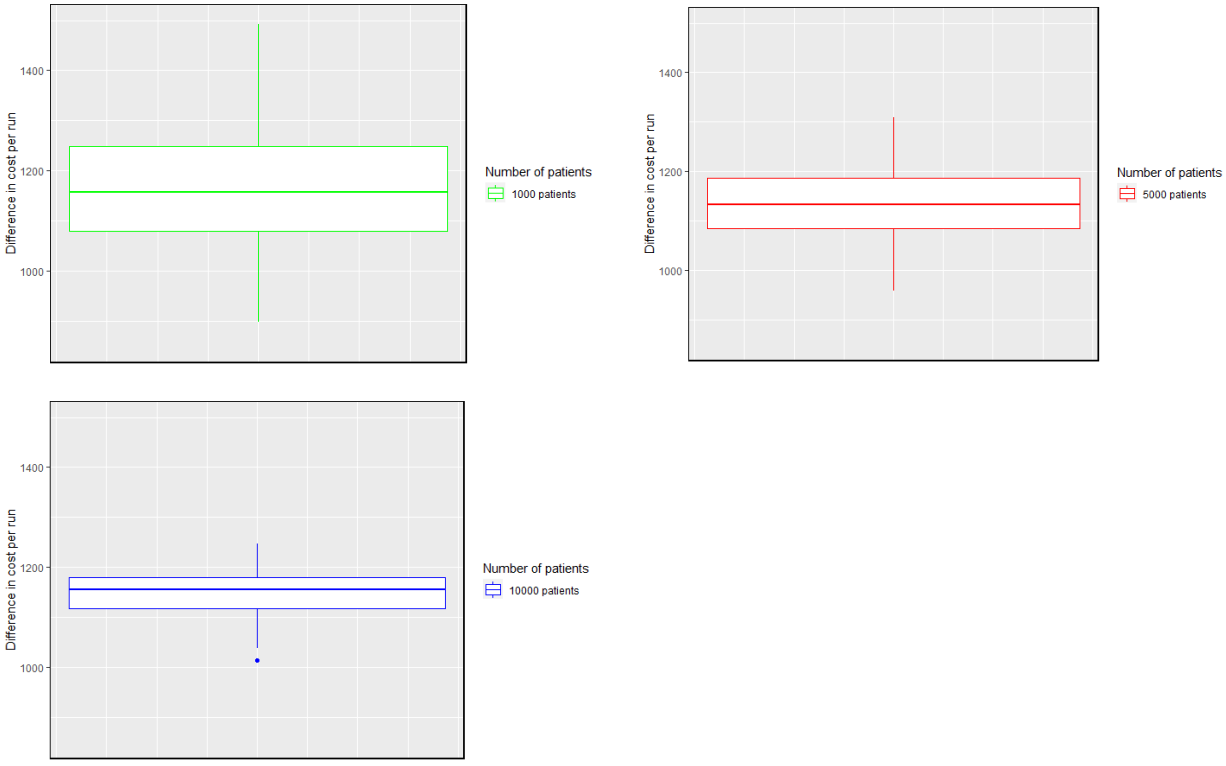

Figure 20: boxplots of difference in costs per number of patients in BCA

Appendix V

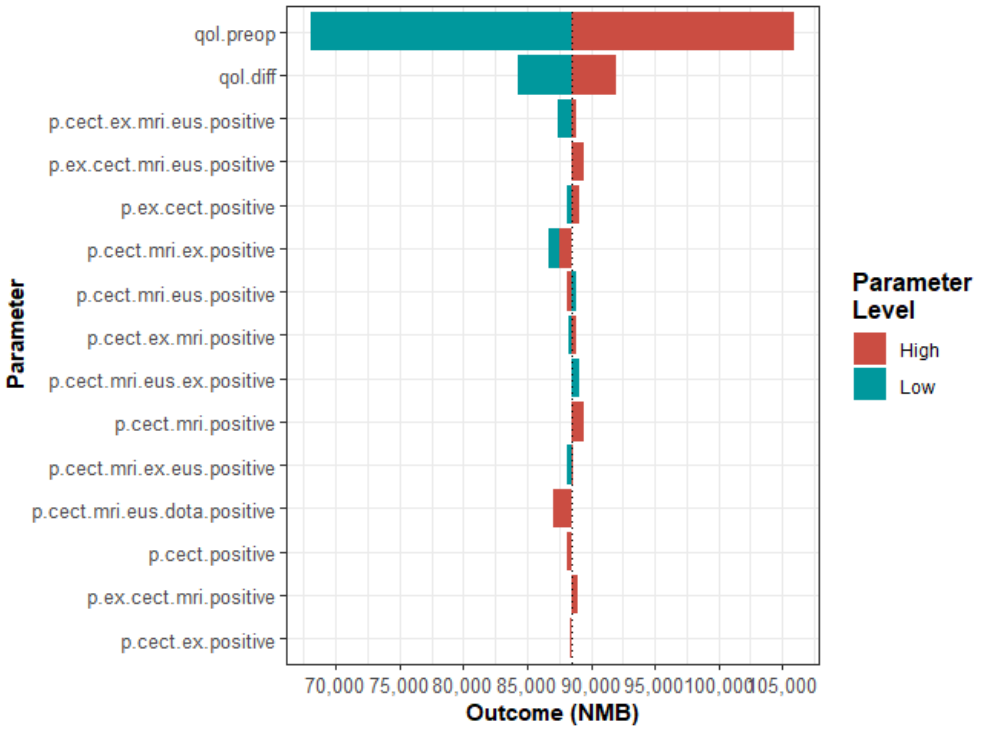

Figure 21: Tornado plot of the impact all model parameters on the NMB outcome of the CT-MRI-EUS-DOTA diagnostic pathway

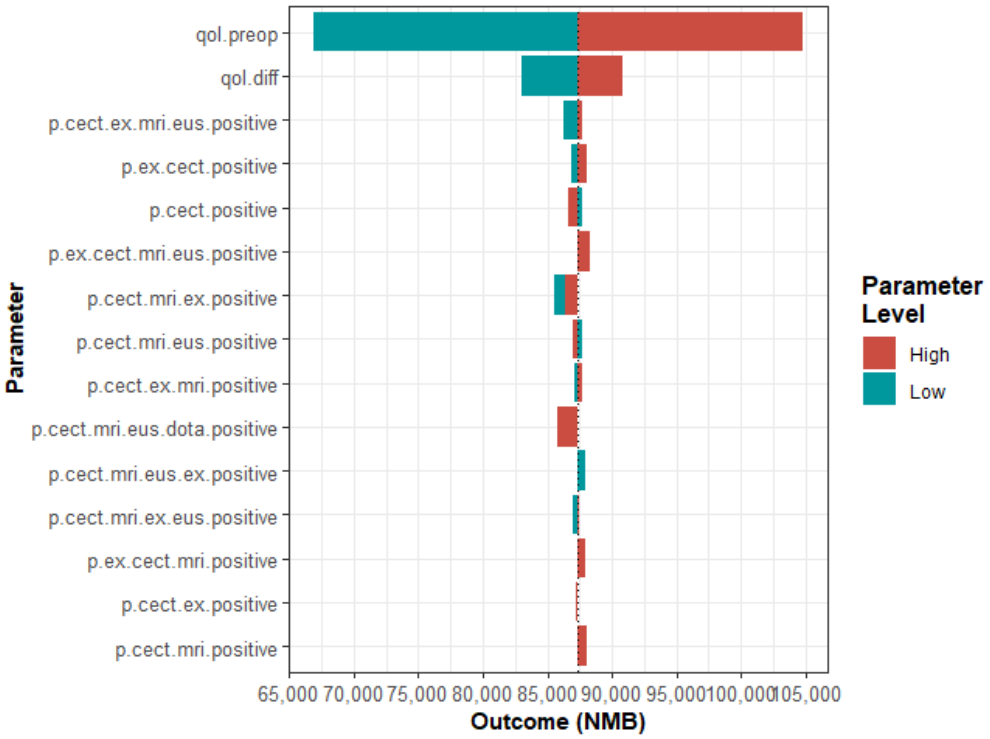

Figure 22: Tornado plot of the impact all model parameters on the NMB outcome of the Exendin+CT-MRI-EUS diagnostic pathway

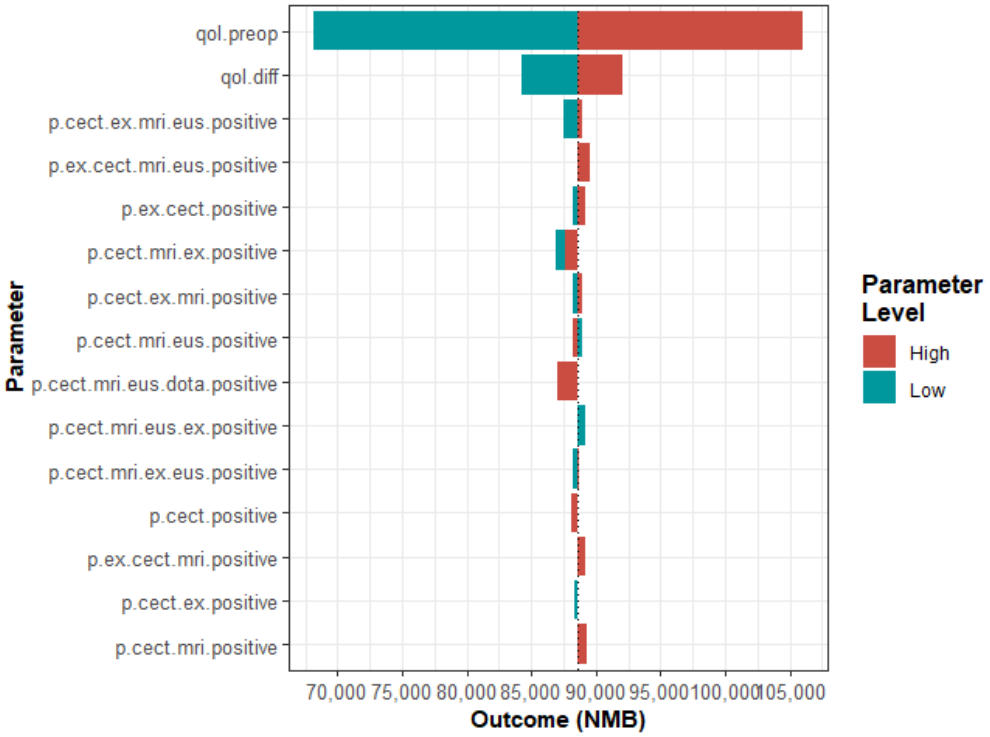

Figure 23: Tornado plot of the impact all model parameters on the NMB outcome of the CT-Exendin-MRI-EUS diagnostic pathway

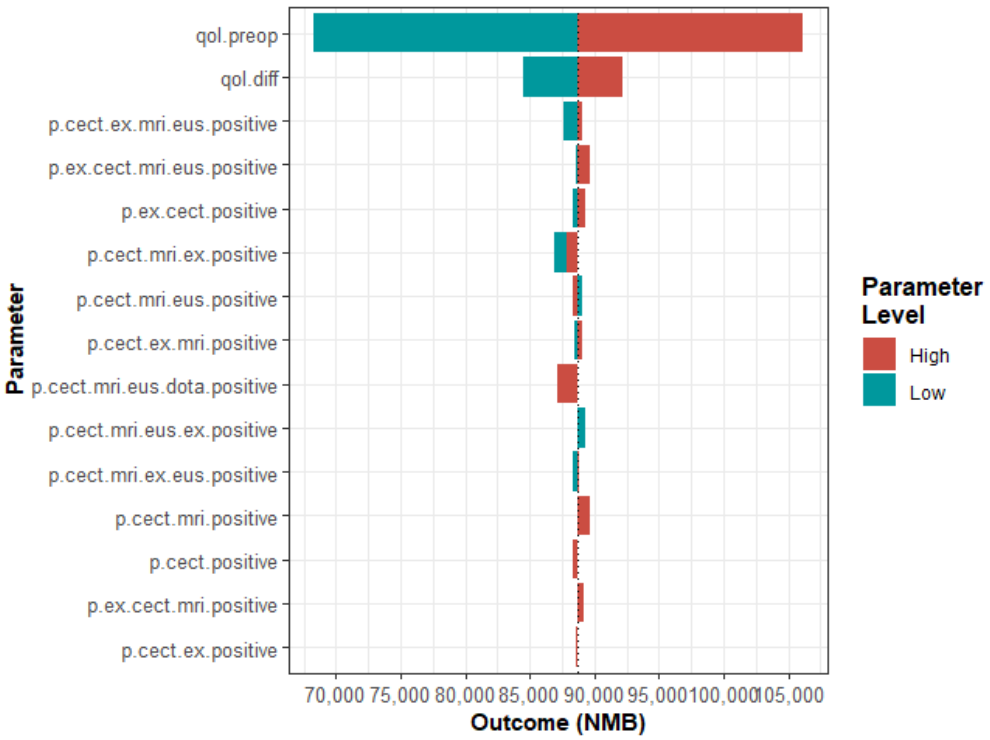

Figure 24: Tornado plot of the impact all model parameters on the NMB outcome of the CT-MRI-Exendin-EUS diagnostic pathway

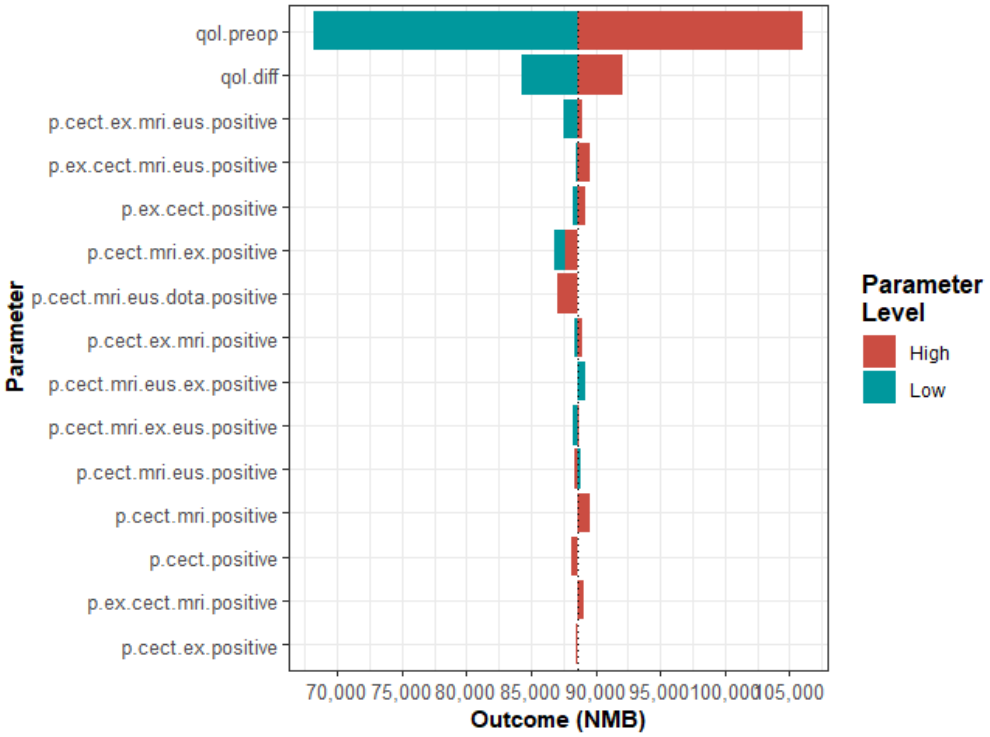

Figure 25: Tornado plot of the impact all model parameters on the NMB outcome of the CT-MRI-EUS-Exendin diagnostic pathway

Appendix VI

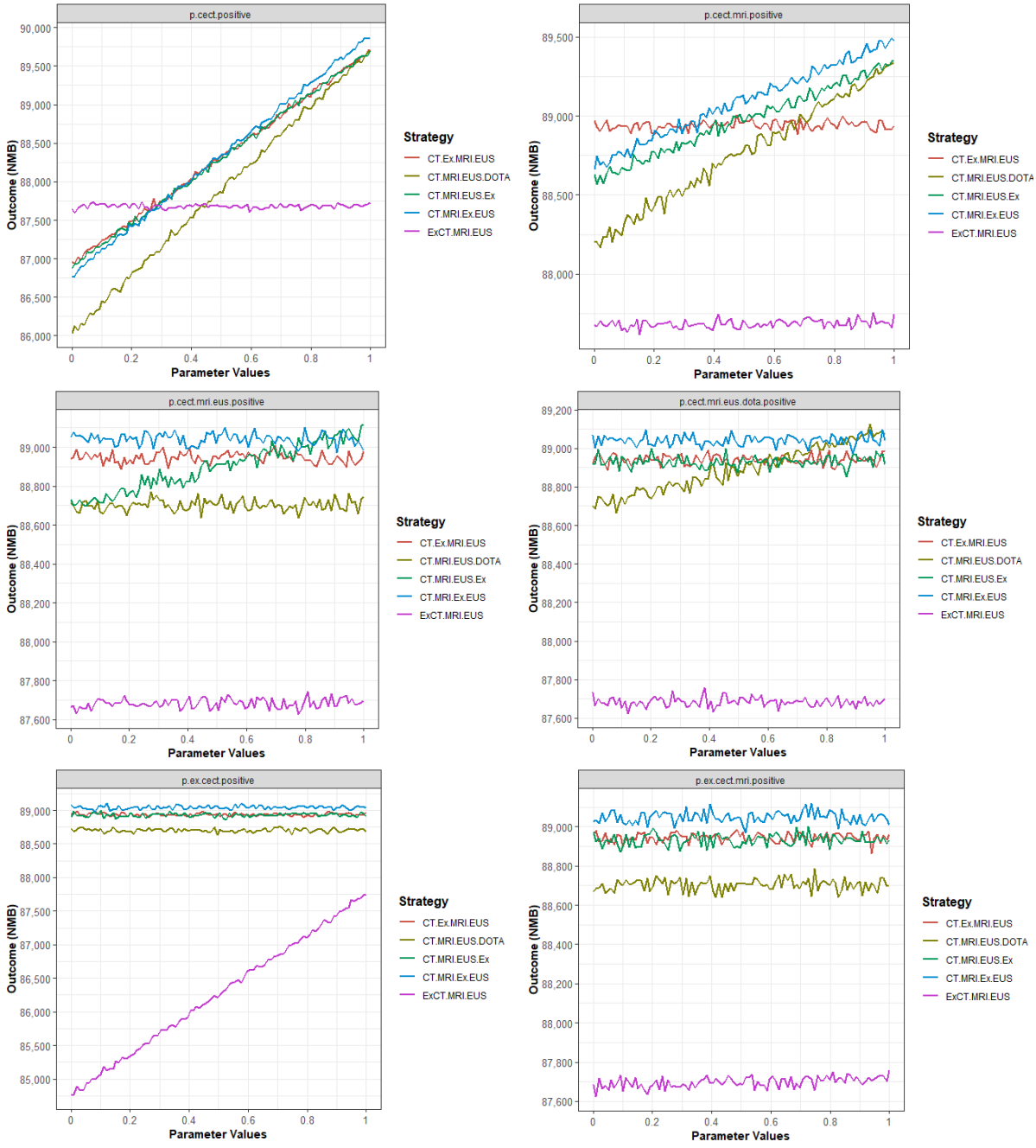

Figure 26: OWSA outcomes of p.cect.positive, p.cect.mri.positive, p.cect.mri.eus.positive, p.cect.mri.eus.dota.positive, p.ex.cect.positive and p.ex.cect.mri.positive

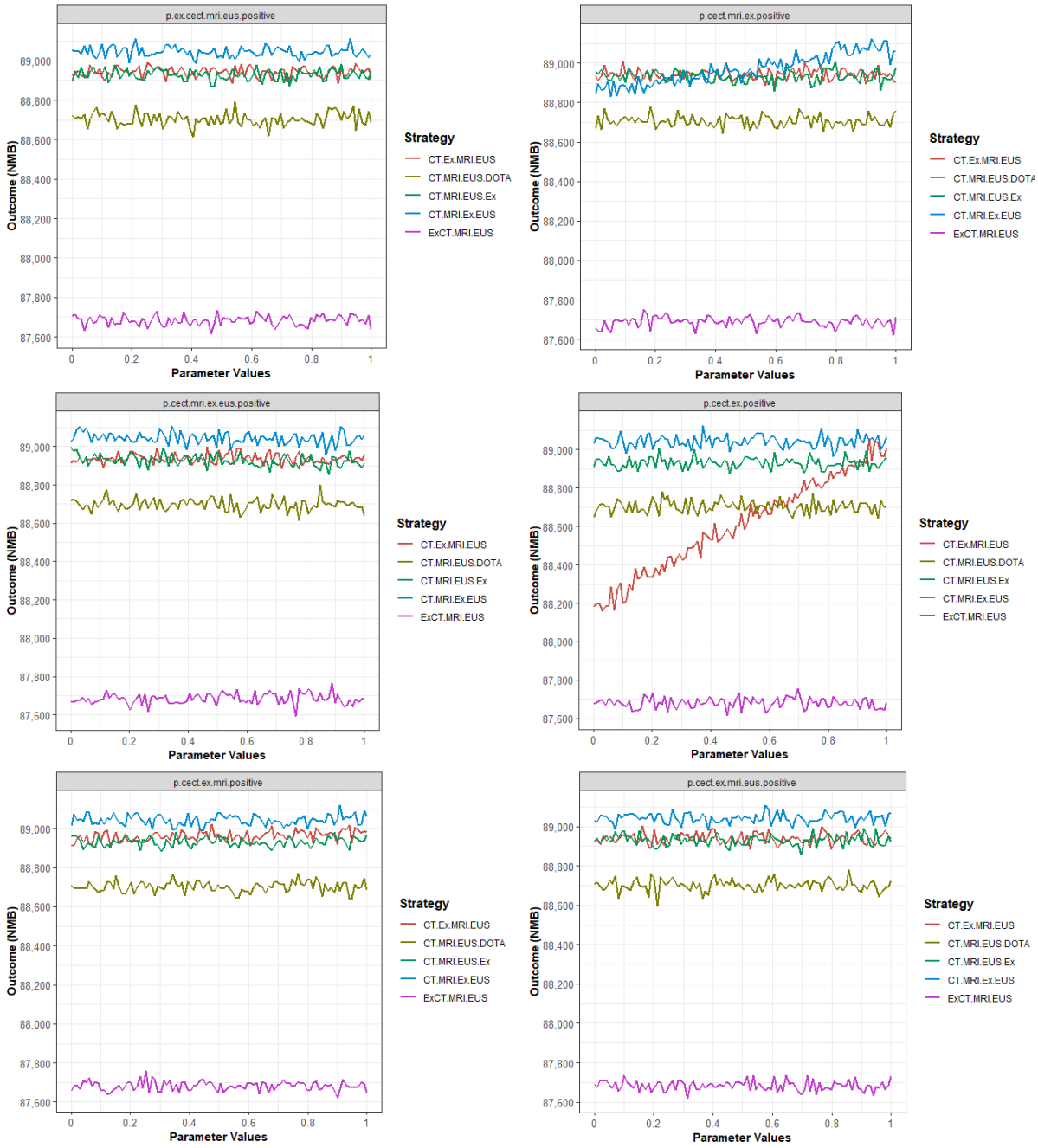

Figure 27: OWSA outcomes of p.ex.cect.mri.eus.positive, p.cect.mri.ex.positive, p.cect.mri.ex.eus.positive, p.cect.ex.positive, p.cect.ex.mri.positive and p.cect.ex.mri.eus.positive

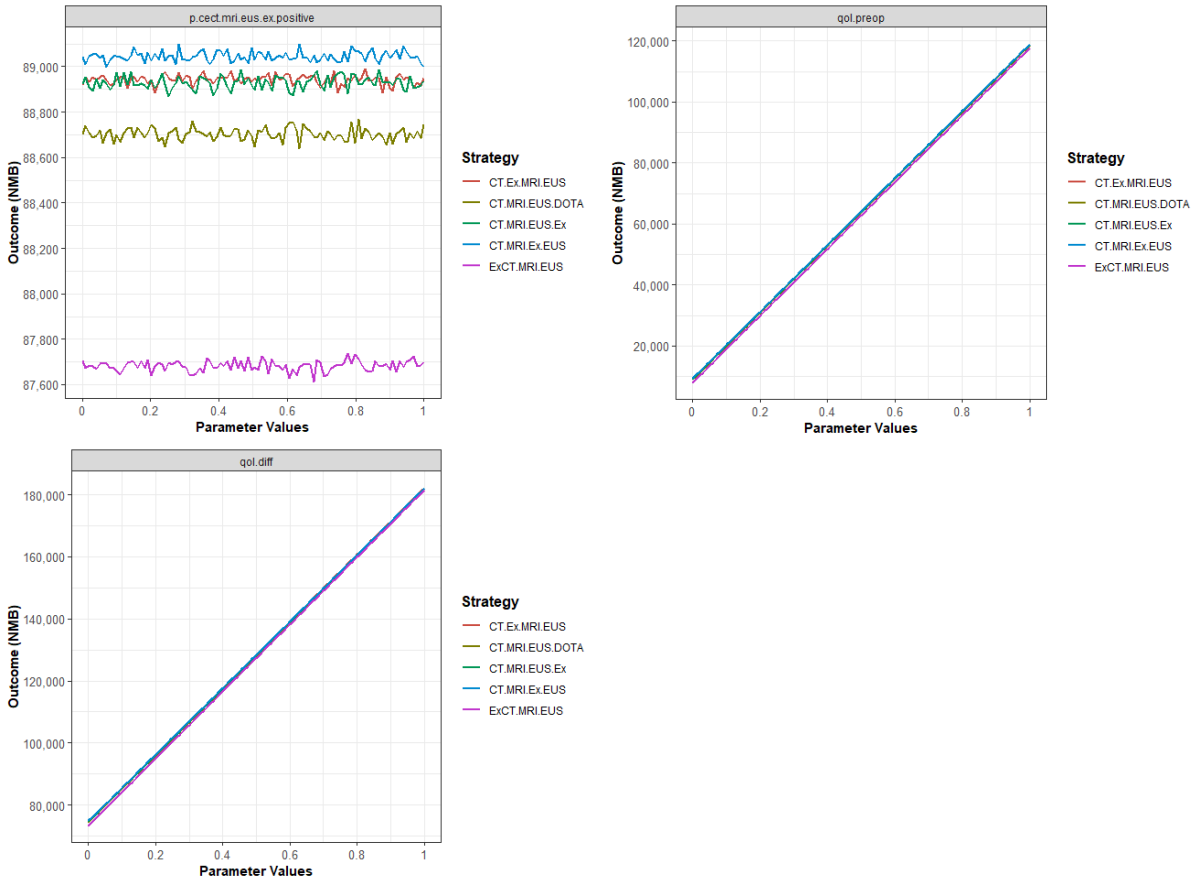

Figure 28: OWSA outcomes of p.cect.mri.eus.ex.positive, qol.preop and qol.diff

Bibliography

Aalbers, R., & Roos, A.-F. (2022). Zorguitgaven, ons een zorg?

Åkerström, G., & Hellman, P. (2007). Surgery on neuroendocrine tumours. *Best Practice & Research Clinical Endocrinology & Metabolism, 21*(1), 87-109.

Boss, M., Mikkola, K., Buitinga, M., Brom, M., Wild, D., Prasad, V., . . . Gotthardt, M. (2019). 68Ga-NODAGA-exendin-4 PET/CT for the localization of insulinomas. *Nuklearmedizin-NuclearMedicine, 58*(02), V31.

Caletti, G., Fusaroli, P., & Bocus, P. (1998). Endoscopic ultrasonography. *Endoscopy, 30*(02), 198-221.

CBS. (2023). Consumentenprijzen; prijsindex 2015=100. Retrieved from https://opendata.cbs.nl/statline/?dl=3F0E#/CBS/nl/dataset/83131NED/table

Changazi, S. H., Ahmed, Q., Bhatti, S., Siddique, S., Raffay, E. A., Farooka, M. W., & Ayyaz, M. (2020). Whipple procedure: a five-year clinical experience in tertiary care center. *Cureus, 12*(11).

Chen, X., Feng, L., Yao, H., Yang, L., & Qin, Y. (2021). Efficacy and safety of diazoxide for treating hyperinsulinemic hypoglycemia: A systematic review and meta-analysis. *PLoS One, 16*(2), e0246463.

Cleveland Clinic. (2021). Insulinoma. Retrieved from https://my.clevelandclinic.org/health/diseases/22217-insulinoma

Cooper, K., Brailsford, S. C., & Davies, R. (2007). Choice of modelling technique for evaluating health care interventions. *Journal of the operational research society, 58*(2), 168-176.

Cox, C. P., Segbers, M., Graven, L. H., Brabander, T., & van Assema, D. M. (2020). Standardized image quality for 68Ga-DOTA-TATE PET/CT. *EJNMMI research, 10*(1), 1-10.

De Herder, W. W., van Schaik, E., Kwekkeboom, D., & Feelders, R. A. (2011). New therapeutic options for metastatic malignant insulinomas. *Clinical endocrinology, 75*(3), 277-284.

Ferrer-Garcia, J., Iranzo González-Cruz, V., Navas-DeSolís, S., Civera-Andrés, M., Morillas-Ariño, C., Merchante-Alfaro, A., . . . Camps Herrero, C. (2013). Management of malignant insulinoma. *Clinical and Translational Oncology, 15*(9), 725-731.

Freemantle, N., Evans, M., Christensen, T., Wolden, M., & Bjorner, J. (2013). A comparison of health-related quality of life (health utility) between insulin degludec and insulin glargine: a meta-analysis of phase 3 trials. *Diabetes, Obesity and Metabolism, 15*(6), 564-571.

Goode, P. N., Farndon, J. R., Anderson, J., Johnston, I. D., & Morte, J. A. (1986). Diazoxide in the management of patients with insulinoma. *World Journal of Surgery, 10*, 586-591.

Goswami, J., Somkuwar, P., & Naik, Y. (2012). Insulinoma and anaesthetic implications. *Indian Journal of Anaesthesia, 56*(2), 117.

Gray, A. M., Clarke, P. M., Wolstenholme, J. L., & Wordsworth, S. (2010). *Applied methods of cost-effectiveness analysis in healthcare* (Vol. 3): OUP Oxford.

Graziadio, S., Winter, A., Lendrem, B. C., Suklan, J., Jones, W. S., Urwin, S. G., . . . Kurowska, K. (2020). How to ease the pain of taking a diagnostic point of care test to the market: a framework for evidence development. *Micromachines, 11*(3), 291.

Hajjarsaraei, H., Shirazi, B., & Rezaeian, J. (2018). Scenario-based analysis of fast track strategy optimization on emergency department using integrated safety simulation. *Safety science, 107*, 9-21.

Hansen, J. B. (2006). Towards selective Kir6. 2/SUR1 potassium channel openers, medicinal chemistry and therapeutic perspectives. *Current medicinal chemistry, 13*(4), 361-376.

Hennrich, U., & Benešová, M. (2020). [68Ga] Ga-DOTA-TOC: the first FDA-approved 68Ga-radiopharmaceutical for PET imaging. *Pharmaceuticals, 13*(3), 38.

Jensen, R. T., Cadiot, G., Brandi, M. L., De Herder, W. W., Kaltsas, G., Komminoth, P., . . . Kianmanesh, R. (2012). ENETS consensus guidelines for the management of patients with digestive neuroendocrine neoplasms: functional pancreatic endocrine tumor syndromes. *Neuroendocrinology, 95*(2), 98-119.

Katz, M., & Erstad, B. (1989). Octreotide, a new somatostatin analogue. *Clinical pharmacy, 8*(4), 255-273.

Kinova, M. (2015). Diagnostics and treatment of insulinoma. *Neoplasma, 62*(5), 692-704.

Landa, P., Sonnessa, M., Tànfani, E., & Testi, A. (2018). Multiobjective bed management considering emergency and elective patient flows. *International Transactions in Operational Research, 25*(1), 91-110.

Marshall, D. A., Burgos-Liz, L., IJzerman, M. J., Osgood, N. D., Padula, W. V., Higashi, M. K., . . . Crown, W. (2015). Applying dynamic simulation modeling methods in health care delivery research—the SIMULATE checklist: report of the ISPOR simulation modeling emerging good practices task force. *Value in health, 18*(1), 5-16.

Mehrabi, A., Fischer, L., Hafezi, M., Dirlewanger, A., Grenacher, L., Diener, M. K., . . . Fard, N. (2014). A systematic review of localization, surgical treatment options, and outcome of insulinoma. *Pancreas, 43*(5), 675-686.

Öberg, K. (2010). *Pancreatic endocrine tumors.* Paper presented at the Seminars in oncology.

Okabayashi, T., Shima, Y., Sumiyoshi, T., Kozuki, A., Ito, S., Ogawa, Y., . . . Hanazaki, K. (2013). Diagnosis and management of insulinoma. *World journal of gastroenterology: WJG, 19*(6), 829.

Patel, S., Lindenberg, M., Rovers, M. M., Van Harten, W. H., Ruers, T. J., Poot, L., . . . Grutters, J. P. (2022). Understanding the costs of surgery: a bottom-up cost analysis of both a hybrid operating room and conventional operating room. *International Journal of Health Policy and Management, 11*(3), 299-307.

Placzkowski, K. A., Vella, A., Thompson, G. B., Grant, C. S., Reading, C. C., Charboneau, J. W., . . . Service, F. J. (2009). Secular trends in the presentation and management of functioning insulinoma at the Mayo Clinic, 1987–2007. *The Journal of Clinical Endocrinology & Metabolism, 94*(4), 1069-1073.

Ramwadhdoebe, S., Buskens, E., Sakkers, R. J., & Stahl, J. E. (2009). A tutorial on discrete-event simulation for health policy design and decision making: Optimizing pediatric ultrasound screening for hip dysplasia as an illustration. *Health policy, 93*(2-3), 143-150.

Raphael, J., Helou, J., Pritchard, K., & Naimark, D. (2017). Palbociclib in hormone receptor positive advanced breast cancer: a cost-utility analysis. *European Journal of Cancer, 85*, 146-154.

Reckers-Droog, V., Van Exel, N., & Brouwer, W. (2018). Looking back and moving forward: on the application of proportional shortfall in healthcare priority setting in the Netherlands. *Health policy, 122*(6), 621-629.

Rehman, A. (2011). Insulinoma—a deceptive endocrine tumour. *JPMA-Journal of the Pakistan Medical Association, 61*(9), 911.

Reubi, J. C., & Waser, B. (2003). Concomitant expression of several peptide receptors in neuroendocrine tumours: molecular basis for in vivo multireceptor tumour targeting. *European journal of nuclear medicine and molecular imaging, 30*(5), 781-793.

Richards, M. L., Gauger, P. G., Thompson, N. W., Kloos, R. G., & Giordano, T. J. (2002). Pitfalls in the surgical treatment of insulinoma. *Surgery, 132*(6), 1040-1049.

Roijen, L., Linden, N., Bouwmans, C., Kanters, T., & Tan, S. (2015). Kostenhandleiding: Methodologie van kostenonderzoek en referentieprijzen voor economische evaluaties in de gezondheidszorg. *Zorginstituut Nederland. The Netherlands: Zorginstituut Nederland*.

Senniappan, S., Shanti, B., James, C., & Hussain, K. (2012). Hyperinsulinaemic hypoglycaemia: genetic mechanisms, diagnosis and management. *Journal of inherited metabolic disease, 35*(4), 589-601.

Stahl, J. E., Roberts, M. S., & Gazelle, S. (2003). Optimizing management and financial performance of the teaching ambulatory care clinic. *Journal of general internal medicine, 18*(4), 266-274.

Tucker, O., Crotty, P., & Conlon, K. (2006). The management of insulinoma. *Journal of British Surgery, 93*(3), 264-275.

Vázquez-Serrano, J. I., Peimbert-García, R. E., & Cárdenas-Barrón, L. E. (2021). Discrete-Event simulation modeling in healthcare: A comprehensive review. *International Journal of Environmental Research and Public Health, 18*(22), 12262.

Vezzosi, D., Bennet, A., Rochaix, P., Courbon, F., Selves, J., Pradere, B., . . . Caron, P. (2005). Octreotide in insulinoma patients: efficacy on hypoglycemia, relationships with Octreoscan scintigraphy and immunostaining with anti-sst2A and anti-sst5 antibodies. *European Journal of Endocrinology, 152*(5), 757-767.

Weinstein, M. C., & Stason, W. B. (1977). Foundations of cost-effectiveness analysis for health and medical practices. *New England Journal of Medicine, 296*(13), 716-721.

York Health Economics Consortium. (2016). Net Monetary Benefit. Retrieved from https://yhec.co.uk/glossary/net-monetary-benefit/

Zorginstituut Nederland. (2015). Kosteneffectiviteit in de praktijk (Cost-effectiveness analysis in practice). *Diemen, The Netherlands: Zorginstituut Nederland*.

Zorginstituut Nederland. (2023). Farmacotherapeutisch Kompas. Retrieved from https://www.farmacotherapeutischkompas.nl/